Stem Cell Reports

Resource



OPEN ACCESS

Platform-agnostic CellNet enables cross-study analysis of cell fate engineering protocols

Emily K.W. Lo,^{1,2} Jeremy J. Velazquez,^{3,4} Da Peng,^{1,2} Chulan Kwon,^{1,2,5} Mo R. Ebrahimkhani,^{3,4,6,7} and Patrick Cahan^{1,2,*}

 $^{1} Department \ of \ Biomedical \ Engineering, Johns \ Hopkins \ University, \ Baltimore, \ MD \ 21205, \ USA$

https://doi.org/10.1016/j.stemcr.2023.06.008

SUMMARY

Optimization of cell engineering protocols requires standard, comprehensive quality metrics. We previously developed CellNet, a computational tool to quantitatively assess the transcriptional fidelity of engineered cells compared with their natural counterparts, based on bulk-derived expression profiles. However, this platform and others were limited in their ability to compare data from different sources, and no current tool makes it easy to compare new protocols with existing state-of-the-art protocols in a standardized manner. Here, we utilized our prior application of the top-scoring pair transformation to build a computational platform, platform-agnostic CellNet (PACNet), to address both shortcomings. To demonstrate the utility of PACNet, we applied it to thousands of samples from over 100 studies that describe dozens of protocols designed to produce seven distinct cell types. We performed an in-depth examination of hepatocyte and cardiomyocyte protocols to identify the best-performing methods, characterize the extent of intra-protocol and inter-lab variation, and identify common off-target signatures, including a surprising neural/neuroendocrine signature in primary liver-derived organoids. We have made PACNet available as an easy-to-use web application, allowing users to assess their protocols relative to our database of reference engineered samples, and as open-source, extensible code.

INTRODUCTION

Key milestones in advancing the field of cell fate engineering (CFE) include the discovery of direct conversion (Davis et al., 1987), the derivation of mouse and human embryonic stem cells (ESCs) (Evans and Kaufman, 1981; Martin, 1981; Thomson et al., 1998), the directed differentiation of ESCs to motor neurons (Wichterle et al., 2002), and the induction of pluripotent stem cells (induced pluripotent stem cells [iPSCs]) (Takahashi and Yamanaka, 2006; Takahashi et al., 2007). Collectively, these and many other advancements have enabled the development of protocols to derive numerous cell and tissue (CT) types. CFE is used in a range of applications, from regenerative medicine to disease modeling, drug discovery, and drug screening (Robinton and Daley, 2012). Because of the potential importance of these applications, the number of investigators and studies generating, optimizing, and applying CFE methods has multiplied rapidly.

Optimizing CFE methods requires evaluation of protocol performance. This is often done empirically by verifying expression of canonical markers at the protein and RNA level (for instance, SERPINA1 and HNFs in hepatocytes [Ma et al., 2013] and TNNT2 in cardiomyocytes [leda et al., 2010]) or through *in vitro* functional assays (for

example, glycogen storage and albumin secretion in hepatocytes, calcium flux and spontaneous beating in cardiomyocytes, sodium currents and spontaneous postsynaptic currents in neurons [Kang et al., 2017], and teratoma formation to assess pluripotency [Brivanlou et al., 2003; Thomson et al., 1998]). The most stringent assays of CFE fidelity entail assessing the extent to which transplanted cells rescue an absent or disrupted *in vivo* function, as exemplified by complementation of tetraploid blastocysts with PSCs (Nagy et al., 1990).

Genome-wide measurements of molecular state, such as transcriptional profiling, are valuable supplements to functional assays of cell identity for two major reasons. First, they are less time consuming and less experimentally challenging to perform. Second, when coupled with appropriate analysis methods, they can reveal molecular programs that have not been reprogrammed appropriately. This feature is especially valuable in cases where engineered cells fail in functional assays. Several computational methods have been devised to take advantage of genome-wide molecular data to evaluate the fidelity of CFE protocols. For example TeratoScore, PluriTest, and ScoreCard assess pluripotency (Avior et al., 2015a; International Stem Cell Initiative, 2018; Müller et al., 2011; Tsankov et al., 2015), and KeyGenes assesses developmental



²Institute for Cell Engineering, Johns Hopkins University, Baltimore, MD 21205, USA

³Department of Pathology, School of Medicine, University of Pittsburgh, Pittsburgh, PA 15213, USA

⁴Pittsburgh Liver Research Center, University of Pittsburgh, Pittsburgh, PA 15261, USA

⁵Department of Medicine, Johns Hopkins University, Baltimore, MD 21205, USA

Department of Bioengineering, Swanson School of Engineering, University of Pittsburgh, Pittsburgh, PA 15261, USA

⁷McGowan Institute for Regenerative Medicine, University of Pittsburgh, Pittsburgh, PA 15219, USA

^{*}Correspondence: patrick.cahan@jhmi.edu



stage using a fetal tissue atlas (Roost et al., 2015). We previously developed CellNet (Cahan et al., 2014; Lo and Cahan, 2019; Radley et al., 2017), which estimates the degree to which CT-specific gene-regulatory networks (GRNs) have been established in engineered cells. A limitation shared by all of the methods mentioned above is that the query data (i.e., the expression profiles from the engineered cells) and the training data (i.e., the profiles of the primary, in vivo populations) must be produced using the same technologies and downstream computational processing methodologies. Another commonality is that they are typically optimized for and deployed in a studyspecific manner. These issues make it challenging to fairly compare CFE products across protocols and studies, which would be necessary to determine the extent to which new CFE protocols improve fidelity compared with standard methods in the field and to investigate intra-protocol variability. To our knowledge, an extensive cross-study comparison of CFE protocols from bulk-derived data for multiple lineages has not yet been performed, and no easy-to-use computational tool with appropriate benchmark data of CFE protocols exists.

To address this deficiency, we leveraged our recent work using the top-scoring pair (TSP) transformation (Peng et al., 2021; Tan and Cahan, 2019) to make a computational tool that assesses the transcriptional fidelity of CFE products in a platform-agnostic manner. Like CellNet, the tool uses nodes in CT GRNs as predictor variables to train a multi-class random forest (RF) classifier. However, distinct from the original versions of CellNet, which were limited to identically preprocessed microarray or bulk RNA sequencing (RNA-seq) data, we leveraged the TSP transform to allow analysis of data derived from distinct genome-wide expression assays (including microarray and Illumina- and ION torrent-based RNA-seq) as well as data derived from distinct methods of preprocessing raw sequencing data into gene expression estimates. Therefore, we named the tool platform-agnostic CellNet (PACNet).

We compiled a database of publicly available bulk human gene expression data from 101 CFE experiments, totaling more than 2,100 samples across seven CT types. Using PACNet, we quantitatively evaluated the most common, most consistent, and best-performing protocols for two of the most commonly engineered tissue types: heart and liver. We identified common off-target signatures across heart and liver engineering protocols and revealed an unexpected neural and neuroendocrine signature in primary liver-derived organoids. Finally, we created a user-friendly web application (http://cahanlab.org/resources/agnosticCellNet_web/) through which investigators can upload gene expression data to evaluate the transcriptional fidelity of their engineered cells to their natural counterparts and can compare their engineered

cells with our database of engineered reference samples from state-of-the-art CFE protocols. Visitors to the site can readily explore the pre-computed PACNet analysis of all 101 CFE datasets, and users can download our database of reference samples and run PACNet locally (https://github.com/pcahan1/PACNet). Optionally, users can also leverage their own reference data, for example, to add additional CT types to the platform. We think that PACNet's ease of use will make it especially valuable as a resource for investigators to rapidly evaluate the efficacy and performance of CFE protocols in a standardized fashion.

RESULTS

PACNet classification is precise and sensitive

To train PACNet, we first mined NCBI GEO for bulk RNAseq profiles of primary, healthy human CT samples from 14 CT types: B cells, endothelial cells, ESCs, fibroblasts, heart, hematopoietic stem and progenitor cells (HSPCs), intestine/colon, kidney, liver, lung, monocytes/macrophages, brain, skeletal muscle, and T cells. This process resulted in more than 1,400 samples across the 14 CT types (Table S1). To enable cross-platform compatibility, PACNet borrows from the previously described TSP algorithm to transform data prior to training and RF classification (Geman et al., 2004; Peng et al., 2021; Tan and Cahan, 2019). We note that the PACNet classification score for a specific CT type is the fraction of decision trees in the RF classifier in which the sample is predicted to be the specified CT. This is distinct from a global measure of similarity, such as the Pearson or Spearman correlation coefficient. Consistent with our prior work, where we used TSP-RF to perform cell typing of single cell atlases (Tan and Cahan, 2019) and to evaluate cancer models from bulk RNA-seq data (Peng et al., 2021), PACNet performed well when applied to held-out samples, with an average classification score (corresponding to the labeled cell type) of 0.965 among all held-out samples, with cell type-specific averages ranging from 0.872 (kidney) to 0.996 (neuron) (Figure 1A). We also evaluated classifier performance via precisionrecall (PR) curves, summarized as area under the PR curve (AUPR). The AUPR among non-random cell types averaged 0.9981 and ranged from 0.9962 (kidney) to 0.9996 (monocyte/macrophage) (Figures S1A and S1B). To validate the platform agnosticism of PACNet, we next queried the bulk RNA-seq-trained classifier with a database of primary human microarray data (Cahan et al., 2014). PACNet successfully classified the vast majority of samples (Figure 1B), with a mean AUPR across all cell types of 0.987 and a minimum AUPR of 0.936 for HSPCs, demonstrating that the classifier maintained high performance across expression profiling platforms.



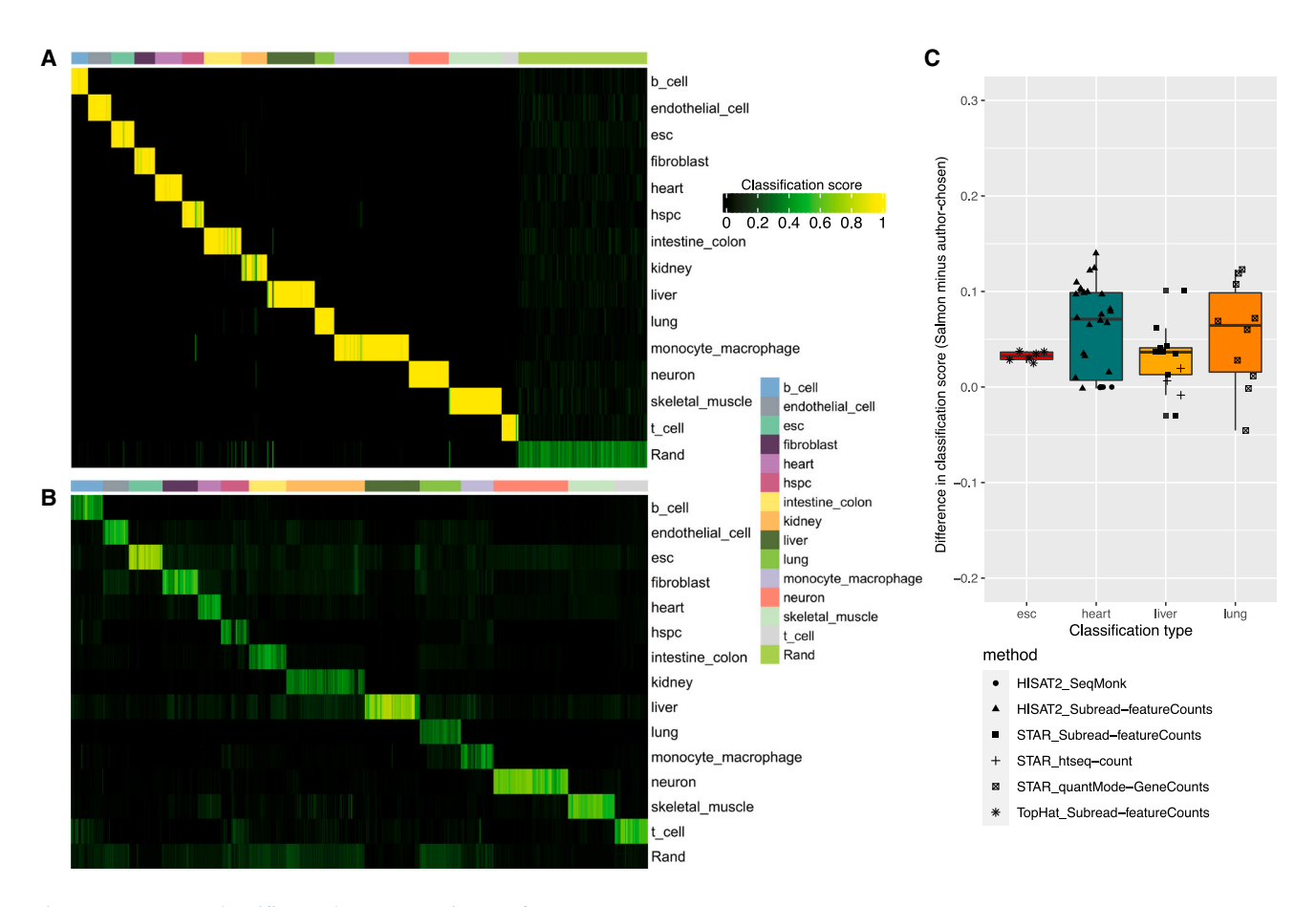


Figure 1. PACNet classifier and preprocessing performance

(A) Heatmap of classification scores of held-out samples for classifier validation. Each column represents a held-out bulk RNA-seq sample. (B) Heatmap of classification scores for primary tissue microarray query data. Each column represents a microarray sample. (A and B) Each row represents a cell/tissue type, and the colors correspond to the classification score, which is the proportion of decicision trees in the Random Forest classifier in which the given sample is classified as the row's CT. Rand: random.

(C) Difference in classification scores based on in-house vs. author-performed RNA-seq alignment and quantification pipelines for CFE studies. Only in vivo positive controls from iPSC, heart, liver, and lung CFE studies were analyzed. Method legend: tools used for author-performed RNAseq alignment and quantification. Mean difference of 0.0495 across all comparisons; no difference in scores was greater than 0.14. See also Figure S1.

To create a reference database of major CFE protocols, we again mined GEO for publicly available bulk gene expression data of engineered human cells. We aimed to identify a variety of protocol types for each CT type, including directed differentiation, transdifferentiation, and organoid derivation protocols. We also sought to compile studies using different expression profiling platforms, including microarray (one study), Illumina-based RNA-seq (vast majority of studies), ION torrent-based RNA-seq (four studies), and GRO-seq (one study). Altogether we gathered 101 CFE experiments for heart (24 studies), HSPCs (5), intestine/colon (12), liver (25), lung (5), neuron (21), and skeletal muscle (9), totaling more than 2,100 samples (Table S2). Because our goal was also to make a metric of CFE that would be well calibrated across studies that use different computational preprocessing methods, we verified that PACNet performance was not affected by variations in alignment and quantification tools or by variations in available genes (Figures 1C and S1B; Table S3; Note S1). We attribute the robustness of PACNet cell fate assessment—against variations in profiling platform, alignment and quantification pipeline, and even counts vs. per-million quantification—to the TSP-RF algorithm because it compares the relative expression of gene pairs within samples rather than absolute or normalized expression among samples.

Cardiomyocytes and hepatocytes are frequently the target of CFE efforts because of their potential applications in toxicity screening and regenerative medicine (Buikema et al., 2013; Jin et al., 2021; Karakikes et al., 2015; Schwartz et al., 2014). In the following sections, we used PACNet to



quantify the transcriptional fidelity of common cardiomyocyte and hepatocyte CFE methods, to quantify the extent and frequency of off-target effects, and to explore the biological pathways that distinguish CFE protocols.

Metabolic selection enhances the transcriptional fidelity of engineered cardiomyocytes

We first identified common derivation protocols among cardiomyocyte (CM) CFE studies (Figure 2A). Two commonly used CM directed differentiation monolayer protocols, which we hereafter denote by the first authors, are the Burridge (Burridge et al., 2014, 2015) and Lian (Lian et al., 2012, 2013) protocols, which comprise the following stages.

- (1) GSK3 inhibition in PSCs with CHIR99021 for 48–72 h to induce mesoderm development.
- (2) Wnt inhibition for 48 h using small-molecule PORCN inhibitors: Wnt-C59 (Burridge) or IWP-2 (Lian) to generate cardiac mesoderm.
- (3) Medium changes with RPMI, L-ascorbic acid 2-phosphate, and albumin (Burridge) or RPMI and B-27 (Lian). Beating or contractile cells are observed on day 7.
- (4) In the Burridge protocol only, on day 10: metabolic selection via glucose deprivation and/or sodium DL-lactate supplementation, based on a finding by To-hyama et al. (2013), which purifies up to 95% TNNT2+ cells.
- (5) Differentiated, contractile CMs generated from both protocols can be maintained in culture for more than 6 months.

Several studies append the metabolic selection step from Burridge to the Lian protocol (Note S2); we designate these as "Combined." Another monolayer protocol is simple, comprising a one-step, 24-h treatment with activin, followed by at least 8 days of culture in only RPMI and B-27 (Estarás et al., 2017; Hsu et al., 2018). We denote these studies as "Activin-based." Alternative protocols by Yang et al. (2008) and Lee et al. (2017), which we denote as "embryoid body" (EB) protocols, use recombinant growth factors in lieu of small molecule inhibitors for differentiation. The EB protocol stages are as follows:

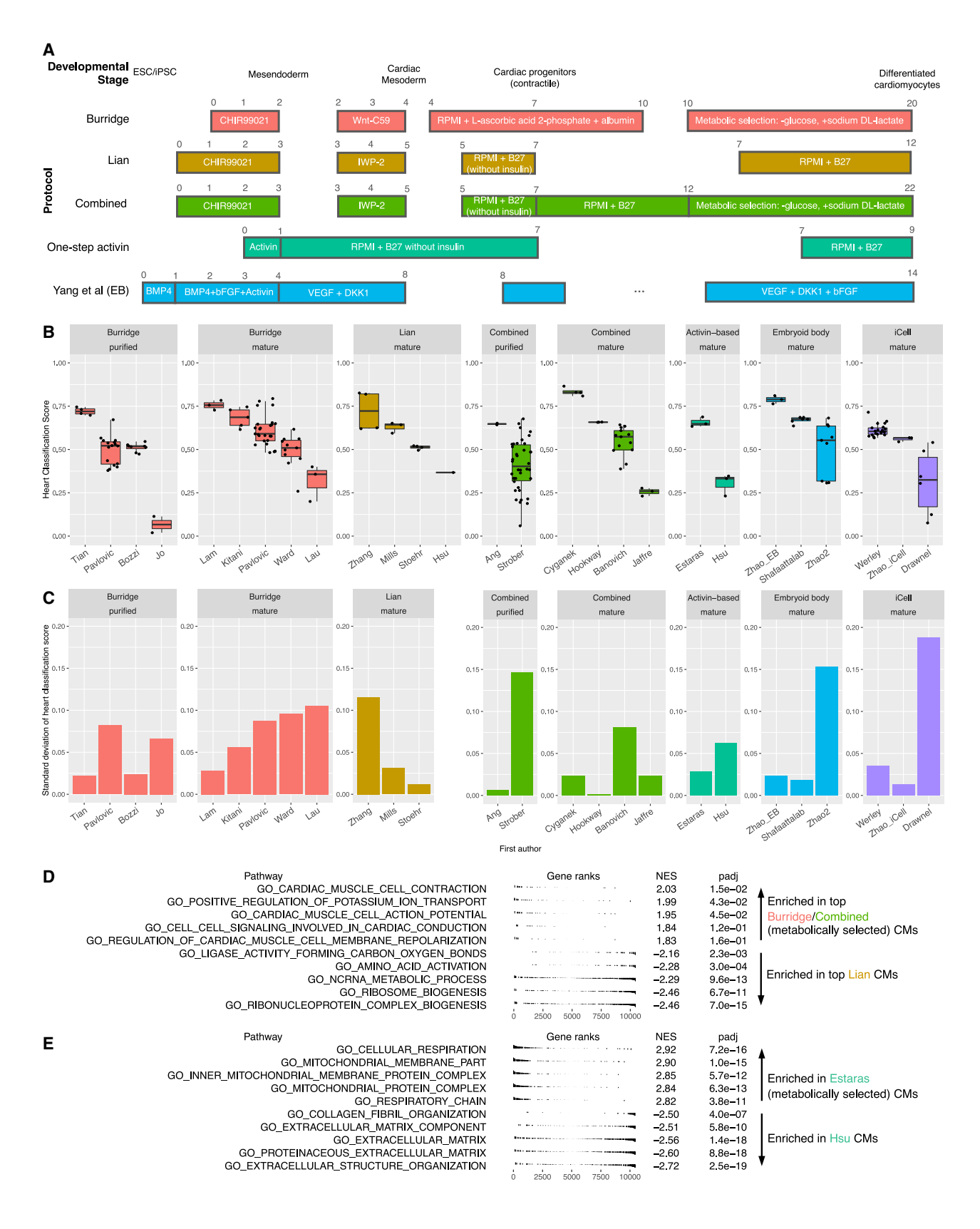
- (1) Formation of EBs from PSCs using BMP4.
- (2) Primitive streak induction using BMP4, bFGF, and activin A.
- (3) Cardiac mesoderm induction using VEGF and Wnt-inhibiting factor DKK1.
- (4) CM specification using VEGF, DKK1, and bFGF.

Finally, we denote commercially purchased CMs as "iCell" CMs.

To assess to what extent these protocols achieved an identity comparable with in vivo CMs, we acquired publicly available bulk expression data as follows: eight studies following the Burridge protocol, four exclusively following the Lian protocol, six combining the Lian protocol with the added metabolic selection step, two following onestep Activin-based protocols, three following EB protocols, and three studies using purchased iCell CMs, for a total of 23 studies and 809 samples across a range of stages of differentiation (Note S2; Table S4). We queried each of these studies with the PACNet classifier (Figure \$1C). Comparing among developmental stages, PACNet analysis showed that most CM protocols demonstrated a gradual, consistent increase in heart classification score and decrease in ESC classification score over their differentiation time courses (Figure S1D). Although increased time in culture was generally associated with a higher PACNet heart classification score, shorter protocols were still able to achieve nearmaximal classification (Figure S1E and S2A; Note S3). Because expression of marker genes has been used as a surrogate for overall transcriptional fidelity, we explored the extent to which PACNet classification score was predicted by expression of individual markers of CM fate. Across samples, we computed the correlation between heart classification scores and the expression of key CM marker genes, including TNNT2, TBX5, and MYL2 (Figure S2B). PACNet heart classification scores correlated substantially with marker expression (R² ranging from 0.35–0.73). However, this correlation was imperfect such that the samples with the highest classification scores (primary heart, as expected) did not have maximal expression of TNNT2 and TBX5. Conversely, samples with maximal marker gene expression (some engineered CMs) did not have the highest classification scores. Therefore, for these samples and marker genes, classification scores better reflect cell identity than the expression of any single marker gene.

We noticed that, even within the same protocol, study, and time point, classification scores of replicates could vary greatly. Intra-lab and inter-lab reproducibility and consistency are important characteristics to consider in CFE; thus, we asked to what extent CMs engineered using the same protocol vary within and across studies. To do so, we computed the PACNet heart classification score for individual studies within and across protocols for "purified" CMs (metabolically selected CMs not yet designated as "mature") from Burridge and combined and all mature CMs (Figure 2B). To facilitate a fair comparison for this and subsequent analyses, we excluded any CMs with disease phenotypes, drug exposure, or genetic perturbations that might obscure accurate assessment of protocol fidelity. In cases where a study had multiple protocol variations, we selected the variant that yielded samples with the highest mean classification score for the target CT. In one notable





(legend on next page)



case, a large study that generated almost 300 samples across 19 independent rounds of differentiation (Strober et al., 2019) produced purified CMs with heart classification scores ranging from 0.016-0.611 (Figures 2B, S1C, and S1D). Other studies with higher variability in classification score included Ward and Pavlovich (Burridge protocol), Banovich (Combined), and Zhao2 (EB) (Figure 2C). The source of this intra-study variation is unclear; however, one likely contributor is PSC line-specific differentiation bias. For example, it is known that independently derived ESC lines can generate unique differentiation biases (Abeyta et al., 2004; Osafune et al., 2008) and that iPSCs can retain epigenetic memory of their initial cell type (Kim et al., 2010). The studies that achieved the highest mean score within their respective protocols often achieved the most consistent scores as well, as in the cases of Tian and Lam (Burridge), Ang (Combined), Estarás (Activin-based), and Shafaattalab (EB) (Figures 2B and 2C). These all generated CMs from an intra-study-consistent starting cell type: Tian and Hookway from fibroblastderived iPSCs, Lam from PBMC-derived iPSCs, and Estarás and Shafaattalab from ESCs. Whereas the highest mean score often achieved the most consistent scores for intrastudy comparisons, inter-study classification scores varied more greatly for all protocols, with a standard deviation (SD) in heart classification score of 0.153 (Burridge) and 0.152 (Combined) for purified CMs and ranging from 0.115 (Lian) to 0.198 (Activin-based) for mature CMs (Figure S2C). The ability of a protocol to produce the most highly classifying CMs did not relate to protocol variability, with comparable top-scoring samples observed in the Lian, Burridge, EB, and Combined protocols irrespective of protocol SD (Figure S2D).

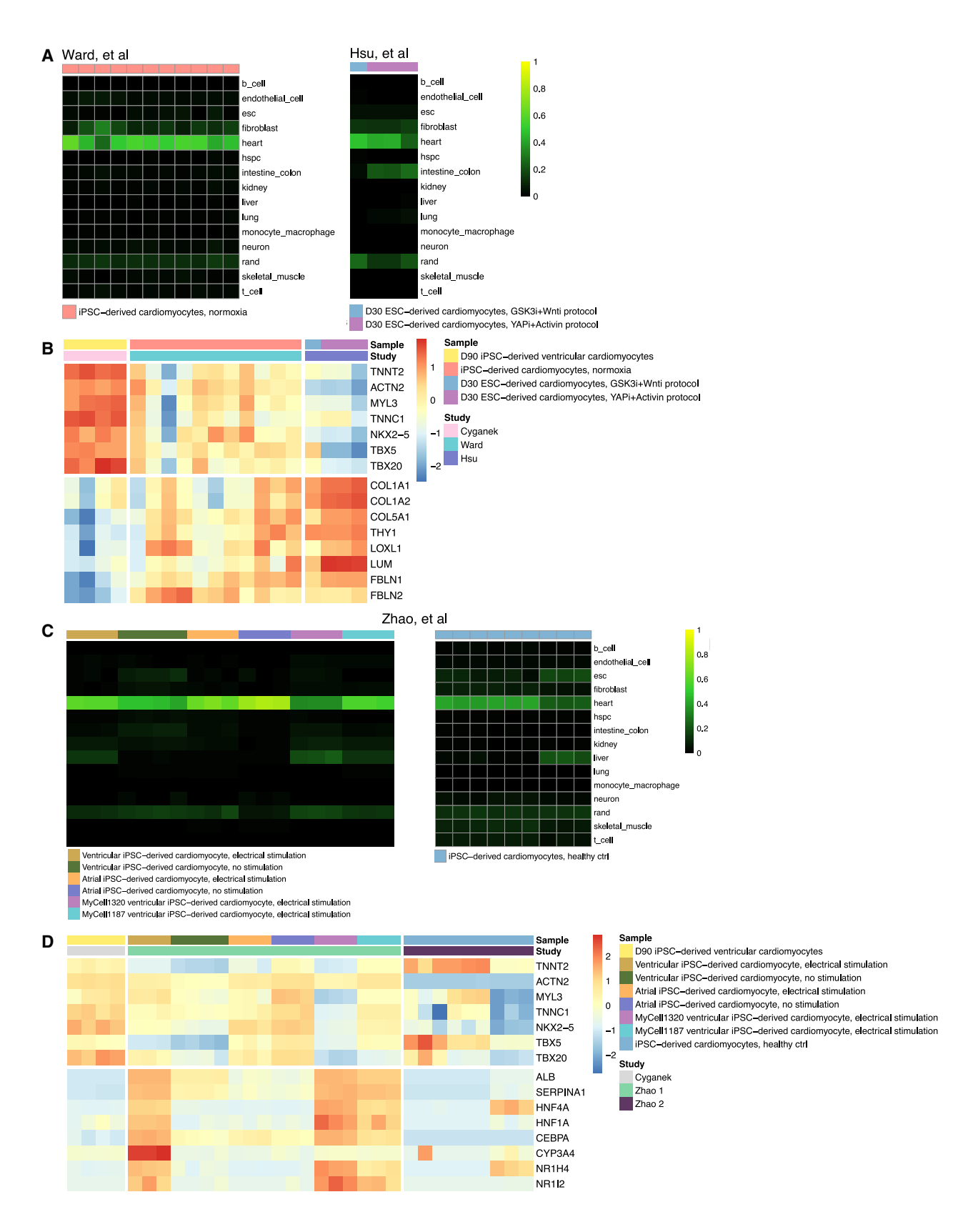
To investigate how differences in protocols contributed to differences in heart classification, we next examined differential expression (DE) among purified and mature CM samples derived via the best-performing study per protocol. We were particularly interested in the effects of metabolic selection on heart classification score because this

step was performed in 15 of 25 studies that produced purified or mature CMs. Thus, we selected the top-classifying Burridge and Combined studies (Tian, Lam, and Cyganek) to compare against the top-classifying Lian studies (Zhang and Mills). We limited the Zhang samples to the two that had not undergone additional study-specific purification via sorting for MYL2 positivity. Gene set enrichment analysis (GSEA) of the DE genes revealed an enrichment in gene sets related to cardiac morphogenesis and action potential in Burridge and Combined samples (Figure 2D), corroborating an increased CM fate in response to metabolic selection. We also examined another relevant comparison within the Activin-based protocol, in which Estarás performed metabolic selection but Hsu did not. GSEA revealed an enrichment of cellular respiration and inner mitochondrial membrane function (oxidative phosphorylation) in the metabolically selected Estarás samples (Figure 2E). This is consistent with the known transition from more glucose- and glycolysis-dependent metabolism during embryonic heart development to more mitochondrion- and fatty acid oxidation-dependent metabolism after birth (Chung et al., 2007; Lopaschuk and Jaswal, 2010). The higher classification scores of metabolically selected mature CMs may reflect this transition away from glycolysis and toward oxidative phosphorylation. Interestingly, we noticed that the two Zhang samples that underwent sorting for MYL2 positivity achieved heart classification scores comparable with the top-classifying Burridge and Combined studies. Thus, we asked whether this sortingbased increase in heart classification scores reflected a common underlying metabolic phenotype. GSEA comparing the Zhang MYL2-sorted samples with top-classifying, non-sorted Lian samples demonstrated an enrichment in cardiac muscle function but surprisingly also in glucose catabolism (Figure S2E). In fact, when comparing against Burridge and Combined samples, we observed the same enrichment in glucose catabolism in the MYL2-sorted Zhang samples (Figure S2F). This suggests that Burridge and Combined samples achieve a strong CM identity

Figure 2. Cross-study meta-analysis of CM engineering protocols

- (A) Schematic of representative protocols in DD of CMs. Protocols are aligned by developmental stage. ESC, embryonic stem cell; iPSC, induced pluripotent stem cell; EB, embryoid body.
- (B) Heart classification scores by study/first author and protocol for healthy/unperturbed purified and mature CM samples (from the topperforming protocol variant, if relevant) per study. Within each facet, studies are ordered by decreasing mean heart classification score. (C) SD in heart classification scores by study/first author and protocol for the same purified and mature CM samples as in (B).
- (D) Summary plot for GSEA performed on DE genes comparing profiles of top-classifying CMs from the Burridge and Combined protocols (Tian, Lam, Cyganek, and Hookway, which include a metabolic selection step) versus top-classifying CMs from the Lian protocol (Mills and Stoehr, which do not include a metabolic selection step). The top 2 classifying samples by Zhang were excluded from this comparison because they were purified using a study-specific method of sorting for MYL2 positivity.
- (E) Summary plot for GSEA performed in DE genes between two Activin-based protocol studies: Estarás et al. (who did perform metabolic selection) to Hsu (who did not). NES, normalized enrichment score; Padj, adjusted p value based on Benjamini-Hochberg correction. See also Figures S1 and S2.





(legend on next page)



through a different mechanism compared with MYL2sorted Zhang samples, which implies a potential for a compounded increase in CM identity when metabolic selection is combined with sorting for MYL2.

It has been observed that directed differentiation and direct conversion can activate transcriptional programs of unintended cell types (Cahan et al., 2014; Kong et al., 2022; Morris et al., 2014). Therefore, we assessed whether there were any off-target lineages detectable in engineered CMs. Although off-target effects were not prominent, we found three minor off-target signatures among CM studies. Two studies showed an aberrant fibroblast signature, although the mature CM samples predominantly still classified as heart (Figure 3A). We corroborated the fibroblast signature with key markers of fibroblast identity, including COL1A1 and THY1 (Figure 3B). The latter of the two studies, Hsu et al. (2018), also showed a noticeable intestinal signature (Figure 3A), which we corroborated with expression of key intestinal genes, including SLC10A2 and MUC2 (Figure S2G). Interestingly, the metabolically selected counterparts (Estarás) to the Hsu CMs lacked both of these off-target signatures (Figure S2H), suggesting that metabolic selection may act to remove off-target cells as well as other cardiac-lineage cells (Andersen et al., 2018; Zhang et al., 2019). A subset of samples from two studies (from the same publication; Zhao et al., 2019) demonstrated an off-target liver signature (Figure 3C), which we corroborated with expression of key liver markers, including ALB, SERPINA1, and CEBPA (Figure 3D). These two studies followed EB protocol variations for CM differentiation (Zhao et al., 2019). It is worth noting that early activation of activin/Wnt signaling also specifies the definitive endoderm adjacent to precardiac mesoderm (Kubo et al., 2004; Toivonen et al., 2013) and endodermal derivatives are often present in cardiac organoids (Drakhlis et al., 2021; Rossi et al., 2021). Thus, these protocols may be permissive to hepatic differentiation as well.

To identify transcription factors (TFs) whose modulation might improve CFE protocol performance, we used the network influence score (Cahan et al., 2014) (NIS) with the minor modification of using rank-transformed

expression estimates instead of quantile-normalized expression estimates. The NIS evaluates the need for up- or down-regulation of cell type-specific TFs based on the expression of those TFs and their target genes. Across engineered mature CMs, NKX2-5 (NK2 homeobox 5) was most strikingly assigned the lowest mean score, indicating a predicted need for upregulation. This is consistent with the role of NKX2-5 as a master regulator of CM fate, controlling a subnetwork of CM TFs, including TBX5, TBX20, HAND1, and HAND2 (Akazawa and Komuro, 2005), which also had moderately strong negative scores (Figure S2I). The NIS successfully prioritized the upregulation of NKX2-5 in CM samples with more prominent off-target signatures (Figure S2I), including Ward (with off-target fibroblasts; Figure 3A). It also recognized the already prominent NKX2-5 activity in highly classifying CM samples, including Cyganek and Zhang (Figures 2B and S2J). Taken together, these results demonstrate the utility of PACNet in assessing crossstudy performance and identifying actionable points for protocol improvement.

Hepatocyte engineering studies have diverse performance outcomes

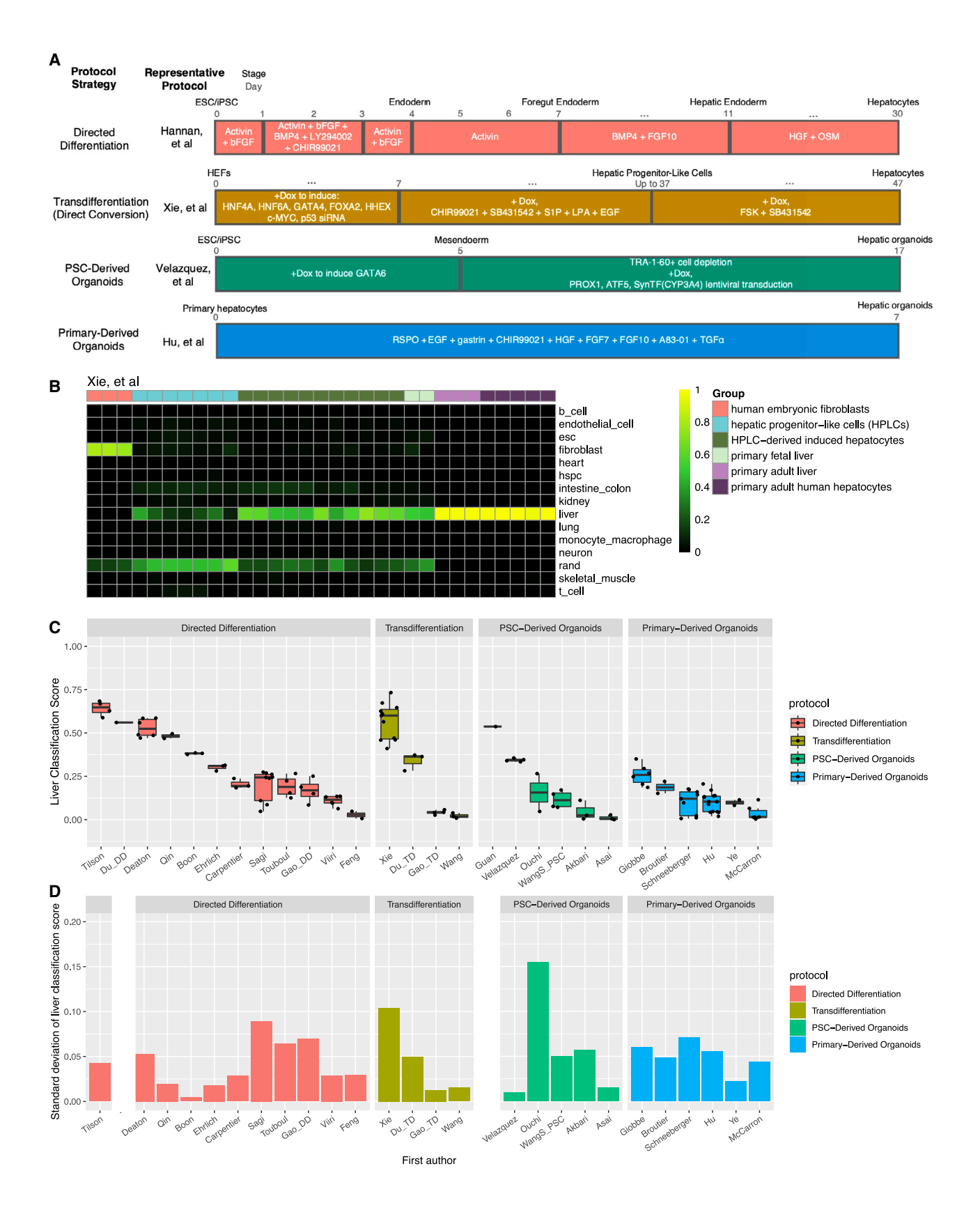
We next identified common hepatocyte (HC) derivation protocols in the field. With less consensus in specific derivation protocols than in CM CFE, we divided hepatic protocols into four general categories: directed differentiation (DD), ESC/iPSC-derived hepatic organoid differentiation (PSC-O), transdifferentiation (TD; i.e., direct conversion), and primary HC-derived or primary liver-derived organoid (P-O) culture. We analyzed 24 studies, divided as follows: 12 DD studies, 6 PSC-O studies, 4 TD studies, and 8 P-O studies (Table S4; Note S4). We summarize each of these derivation strategies below (and illustrate a representative protocol for each in Figure 4A).

- (1) DD protocols followed an overall consistent pattern:
 - (a) Unanimous induction of definitive endoderm from PSCs with activin A, with some adding Wnt3a or BMP4.

Figure 3. Off-target signatures in CM engineering

- (A) Heatmap of classification scores for Ward et al. (left) and Hsu et al. (right) studies, which produced CMs with an off-target fibroblast
- (B) Heatmap of gene expression for canonical CM and fibroblast marker genes for the study with the most highly classifying CMs (Cyganek et al.) compared with the Ward et al. and Hsu et al. studies.
- (C) Heatmap of classification scores for two separate GEO accession studies from the same authors (Zhao et al.), which produced CMs with an off-target liver signature. Heatmap color scale: Z score of log-transformed gene counts.
- (D) Heatmap of gene expression for canonical CM and liver marker genes for the study with the most highly classifying CMs (Cyganek et al.) compared with Zhao et al. studies.
- (B and D) Heatmap color scale: per-gene Z score of log-transformed TPM. See also Figure S2.





(legend on next page)



- (b) Inducing the transitions from definitive endoderm to foregut or hepatic endoderm followed two major strategies: application of BMP4 and FGF2 (Boon et al., 2020; Deaton et al., 2018; Qin et al., 2016) or of 2-mercaptoethanol and DMSO (Carpentier et al., 2020; Ehrlich et al.; Sagi et al., 2019). Other strategies included BMP4 combined with transforming growth factor β (TGF- β) inhibition and Wnt inhibition (Touboul et al., 2016).
- (c) Differentiation to hepatoblasts and HCs or HClike cells was, with large consensus, induced with some combination of oncostatin M. dexamethasone, and HC growth factor (HGF).
- (2) PSC-O protocols followed global strategies similar to DD, but with the addition of various common organoid-promoting factors, including R-spondin1, epidermal growth factor (EGF), Noggin, FGF10, and gastrin (Huch et al., 2013; Pleguezuelos-Manzano et al., 2020) at various stages. Two studies incorporated the TGF-β inhibitor SB431542 and the adenylyl cyclase activator forskolin (Akbari et al., 2019; Wang et al., 2019) during specification to mature hepatic organoids, with one distinct study also adding BMP7 and the Notch signaling inhibitor DAPT during this final stage (Akbari et al., 2019). A unique organoid protocol achieved differentiation through transduction of the transcriptional regulators (TFs) GATA6, PROX1, and ATF5 as well as CRISPR-mediated activation of endogenous CYP3A4 (Velazquez et al., 2021).
- (3) Direct conversion or TD of fibroblasts into HCs involved transduction of specified hepatic TFs, most commonly a combination of HNF family and FOXA family TFs, followed by culture in HC induction medium (Du et al., 2014; Gao et al., 2017; Xie et al., 2019). One unique TD method reverted gastric epithelial cells to an endodermal progenitor state using a cocktail of small-molecule inhibitors, followed by a standard HC differentiation procedure (Wang et al., 2016).
- (4) In P-Os, two major protocols, which we hereafter denote by first author, were used: Huch (Huch

et al., 2015) and Hu (Hu et al., 2018). Huch established a system to expand adult bile duct-derived bipotent liver progenitor organoids, which, upon supplementation with additional factors, can give rise to HCs. Hu then elaborated on this system to establish long-term expansion conditions specifically for HC-derived organoids.

We first assessed to what extent these protocols achieved an identity comparable with in vivo HCs using the PACNet classifier (Figure S3A). Whereas engineered CMs had shown a consistent gradual increase in heart classification score over the course of differentiation, engineered HCs generally experienced a late, sharp increase in liver classification score in the transition from hepatic progenitor to mature HCs (Figures S3B and S3C). Studies demonstrated a concurrent decrease in ESC classification score (or fibroblast classification score for relevant TD studies), although most samples retained a detectable ESC signature (Figures S3B and S3C). Like with CM studies, the correlation between expression of HC markers and liver classification score was again imperfect such that many engineered samples with maximal marker gene expression had only low or moderate classification scores, again suggesting that the classification score better reflects identity than does the expression of select marker genes (Figure S3D).

Next, we asked which protocols produced populations with the highest PACNet classification score. The highestclassifying mature HCs were produced by Xie (Figures 4B and 4C), who used a two-step, 37- to 47-day TD protocol. This protocol first converts embryonic fibroblasts into hepatic progenitor cells through transduction of HNF4A, HNF6A, GATA4, FOXA2, and HHEX, followed by differentiation into functionally competent mature HCs using forskolin and the ALK5 inhibitor SB431542. Almost equally well classifying were two DD studies performed by Tilson and Deaton (Figures 4C, S4A, and S4B), which followed adaptations of a protocol by Hannan et al. (2013) for HC-like cell derivation. While Tilson followed the Hannan method of including the phosphatidylinositol 3-kinase (PI3K) inhibitor LY294002 during definitive endoderm induction, Deaton used a commercially available definitive endoderm

Figure 4. Cross-study meta-analysis of HC engineering protocols

- (A) Schematic of representative protocols from each HC derivation strategy. HEF, human embryonic fibroblast; SynTF(CYP3A4), synthetic TF for endogenous CYP3A4 activation.
- (B) Classification heatmap for the study that produced the most highly classifying HC samples (Xie et al.; TD from human embryonic fibroblasts to HCs).
- (C) Liver classification scores by study/first author and protocol for healthy/unperturbed, fully mature, or differentiated HC and hepatic organoid samples (from the top-performing protocol variant, if relevant) per study. Within each facet, studies are ordered by decreasing mean liver classification score.
- (D) SD in liver classification scores by study/first author and protocol for the same HC or hepatic organoid samples as in (C). See also Figures S3 and S4.



kit. Deaton also uniquely included the myosin II inhibitor blebbistatin during induction of hepatic endoderm from definitive endoderm. Finally, a DD protocol performed by Qin that included supplementation of vitamin K2, known to contribute to HC maturation (Avior et al., 2015b) and to increase expression of mature HC gap junction protein GJB1 (Qin et al., 2016), also had one of the highest mean classification scores (Figures 4C and S4C).

We next examined intra- and inter-study variability in classification score and their relationship to study performance. To facilitate a fair comparison, we again excluded engineered samples with conditions or perturbations that were unrelated to protocol improvement, and when a study had multiple protocol variations, we again selected the variation producing the more highly classifying samples. In CMs, we had observed that intra-study consistency increased with higher mean heart classification score. In contrast, for HC derivation overall, SD was not associated with mean PACNet classification, and low SD did not reflect high protocol performance (Figures 4C, 4D, and S4D). Only the Tilson DD study had a mean classification of over 0.5 while maintaining an SD under 0.05. The Xie study, which did have a mean classification score of over 0.5, had a higher SD of 0.089. Of the PSC-O and P-O studies, Velazquez and Giobbe, respectively, had the highest mean classification scores while maintaining SDs under 0.05 (Figures 4C and 4D). At the inter-study level, while DD and TD protocols had higher SDs of 0.259 and 0.190 respectively, DD and TD samples significantly outperformed P-O and PSC-O samples on average (Figure S4E). The extent to which inter-study and inter-protocol variability in PACNet score reflect functional variability in engineered populations is unknown. Nonetheless, having a quantitative metric of population quality will be useful because the field places more emphasis on reducing variability within protocols.

We next wanted to investigate to what extent DD and TD protocols might each have independent qualities that could help improve the other. To this end, we performed DE analysis and GSEA on mature samples from the most highly classifying DD study (Tilson) and the most highly classifying TD study (Xie). GSEA revealed, in Xie-derived HCs, a slight enrichment of genes involved in liver-related functions, including fatty acid metabolism (CYP4A11 and EHHADH) and bile acid metabolism (NR1I2, NR1H4, and SLC27A5). On the other hand, the Tilson-derived HCs demonstrated a slight enrichment of genes (including PROS1, FGG, FGA, and F9) related to the blood coagulation system, in which HCs are known to play a role (Kopec and Luyendyk, 2014; Figure S4F). Therefore, approaches that leverage aspects of both protocols could lead to additive increases in HC identity. We also again investigated liver-specific TFs whose modulation might improve classification performance using the NIS, which successfully prioritized upregulation of the key liver TF NR1H4 in engineered samples with modest liver classification scores and prominent off-target scores (Figures S4G, S4H, and S5A–S5C; Note S5).

We finally explored off-target signatures in engineered HCs, which were more prevalent than in CM CFE studies (Figures S1C and S3A). PACNet was able to identify the signatures of supporting cell types included during co-culture in two HC derivation studies (Figures S5B and S5D; Note S6). PACNet also detected a consistent aberrant intestine/ colon classification score in several PSC-O and P-O studies (Figure 5A). This was unsurprising given the shared endodermal lineage of intestine and liver and because of shared culture medium components with intestinal organoid culture protocols, including R-spondin1 and EGF (Pleguezuelos-Manzano et al., 2020). Expression of intestinal marker genes, including CDX1, CDX2, and SI, confirmed the offtarget classification (Figure 5B). Interestingly, the samples derived from different studies seemed to express some mutually exclusive intestinal markers, suggesting further specification into intestinal cell subtypes. Upon examination of specific subtype markers, most studies showed some enterocyte and goblet cell lineage enrichment, with McCarron samples being most consistently enriched in these markers. Ouchi samples had a slight tuft cell enrichment based on expression of markers DCLK1 and NREP, while Akbari and Ye samples had increased expression of enteroendocrine (CHGA, NEUROD1, and NKX2-2) and tuft cell markers (Figure 5B). This intriguingly suggests potential avenues for intestinal subtype-specific cell derivation protocols.

Primary liver-derived organoids exhibit consistent offtarget neural signatures

Surprisingly, we observed that several studies of P-Os and one PSC-O study (Hu, Giobbe, Artegiani, and Akbari) showed an unexpected aberrant neuronal classification (Figure 6A) that is absent in samples from healthy human liver (Figures 1A and 5A). Thus, we more closely examined what might contribute to this off-target signal. We confirmed expression of canonical neural marker genes, including PAX6, SOX1, NEUROD1, NEUROD4, and ASCL1 (Figure 6B), and of key neuronal genes from the PACNet classifier (Figure S6A; Table S5) in samples that had neuronal classification. To further investigate this observation and avoid potential batch effects that might arise when integrating gene expression estimates from multiple studies, we analyzed data from the Giobbe study alone. In this study, PACNet analysis indicated that HC organoids cultured in "standard hydrogel" had a stronger liver signature and weaker neural score, while organoids cultured in "ECM hydrogel" had a stronger neural score and a negligible liver score (Figure S6B). GSEA on DE genes between



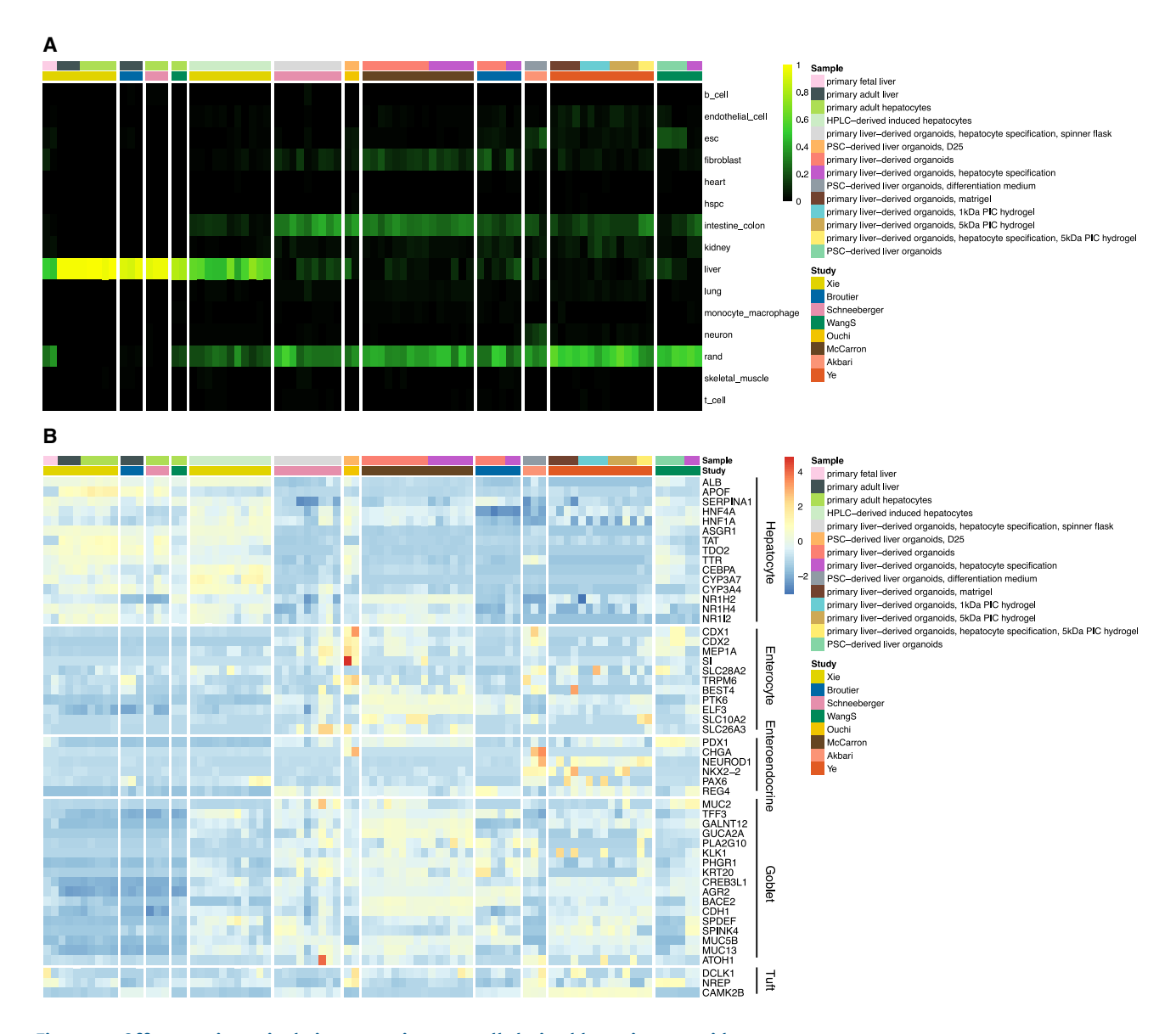


Figure 5. Off-target intestinal signatures in stem cell-derived hepatic organoids

- (A) Classification heatmaps for highest-classifying HC derivation study (Xie et al.) vs. Broutier et al., Schneeberger et al., Wang S et al., Ouchi et al., McCarron et al., Akbari et al., and Ye et al.
- (B) Heatmap of HC and intestinal (split into subcategories) marker gene expression for the same studies as in (A). Heatmap color scale: per-gene Z score of log-transformed TPM. See also Figure S5.

HC organoids cultured in ECM vs. standard hydrogel identified an enrichment of neocortex genes in the former, including *ASCL1*, *NEUROD4*, and *SLC17A6*, and an enrichment of liver-specific genes in the latter, including *ALB*, *SERPINA1*, and *HNF4A* (Figure S6C). The independent detection of brain-related genes sets by GSEA in samples that had a neuronal PACNet classification further corroborates our observation of aberrant neural transcriptional programs in some HC organoids. We noted that the pri-

mary adult and fetal HC positive control samples provided in the Hu study also showed aberrant neuronal classification and expression of neural marker genes (Figures 6A and 6B), potentially suggesting a technical issue with the classifier. However, PACNet successfully classified primary fetal liver, adult liver, fetal HC, and adult HC samples from many other studies (Asai, Boon, Du, Gao, Qin, Schneeberger, Touboul, Viiri, WangS, and Xie) as liver and not neural (Figures S3B and S6D). Therefore, the



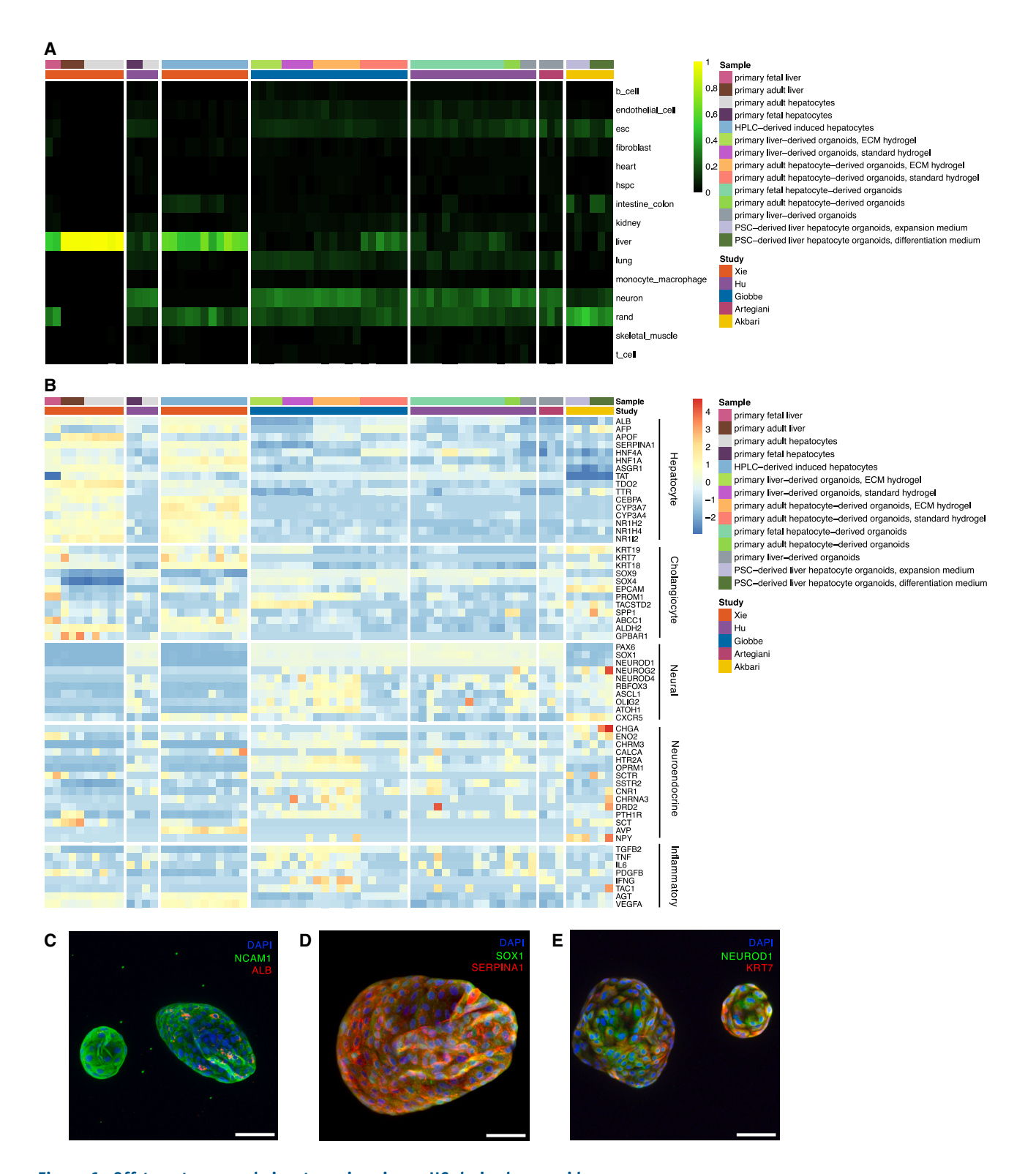


Figure 6. Off-target neuronal signatures in primary HC-derived organoids

(A) Classification heatmaps for the highest-classifying HC derivation study (Xie et al.) vs. Hu et al., Giobbe et al., Artegiani et al., and Akbari et al.

(legend continued on next page)



aberrant neural signature seen in primary samples from the Hu study are unlikely to be due to classifier performance but, rather, potentially arose from inadvertent misannotation of some organoid samples as "primary". Finally, we note that not all P-O samples had this aberrant neural signature; P-O samples generated by Schneeberger, Ouchi, McCarron, Broutier, Ye, and WangS also lacked neuronal classification (Figure 5A). This prompted us to look for differences in derivation strategies that might explain the origin of the neural signature.

P-Os fell into two broad protocols: (1) derivation of bipotent progenitor organoids from EPCAM+ cholangiocytes (WangS, Giobbe subset), followed by an HC specification step (Huch, Schneeberger) and (2) direct derivation of organoids from HCs (Hu, Giobbe subset). The former category also included a variation where bipotent progenitor organoids were initially supplemented with Wnt-conditioned medium and Noggin (Artegiani), followed by the same HC specification step (Broutier). We summarized these protocol differences in Figure S6E. The presence of a neural signature in only Artegiani, Hu, and the Giobbe direct HC subset potentially implicates two mechanisms of origin: (1) culture conditions specific to the Wnt-conditioned medium- and nogginsupplemented bipotent progenitor organoid stage or (2) culture conditions specific to the Hu protocol. Further studies will be necessary to identify the exact determinants of this signature.

We next investigated whether the observed neural signature was connected to related lineages with known liver roles. Neuroendocrine (NE) factors are known to be expressed during ductular reaction (DR) in cholangiopathies (Alvaro et al., 2007; Banales et al., 2019; Ehrlich et al., 2018; Munshi et al., 2011). We hypothesized that NE gene expression might contribute to the neural signature and indeed observed that the aberrant samples also consistently expressed high levels of several NE genes and neuropeptides, including CHGA, CHRM3, and PTH1R, relative to the most highly classifying HC samples generated by Xie (Figure 6B). Liver ductal organoids derived by Giobbe and PSC-Os derived by Akbari also expressed high levels of cholangiocyte (CL) marker genes, including KRT19, EPCAM, PROM1, and TACSTD2. Furthermore, the CL marker SOX9 was also moderately expressed across most aberrant neural samples, although SOX9 is also a broad marker of neural stem cells (Scott et al., 2010), astrocytes (Sun et al., 2017), and intestinal

cells (Blache et al., 2004). Interestingly, although they had the least expression of neural/NE marker genes, Xie engineered HCs had the highest expression of CL markers, including KRT18 and KRT7. We also examined inflammatory markers indicative of DR, including TGFB2 and IL6 (Ehrlich et al., 2018), and found that their expression was indeed generally associated with neural and NE gene expression, particularly in Giobbe ductal organoids and standard hydrogel HC organoids. The fact that many neurally classifying organoid samples did not express CL markers (and that many Xie non-neurally classifying samples expressed CL markers) suggests that DR may be insufficient to fully explain the observed neural/ NE signatures. Nonetheless, DR may contribute to these signatures given that, within the organoid samples, many with the highest neural/NE expression (Giobbe ductal organoids and Akbari PSC-derived HC organoids) also had the highest CL marker expression.

To test whether the aberrant neural/NE signature in cultured P-Os could be recapitulated, we generated organoids from primary human liver using established protocols (Broutier et al., 2016; Huch et al., 2015). We performed immunofluorescence (IF) staining for the HC markers albumin (ALB) and SERPINA1, the CL marker KRT7, the NE marker NCAM1, and the neural markers SOX1 and NEUROD1. We observed very little ALB expression (Figures 6C and S6F), consistent with a lack of mature HC identity, while the early HC marker SERPINA1 was more abundant (Figures 6D and S6F). KRT7 was detectable (Figures 6E and S6F), consistent with a ductal-like biliary phenotype (Huch et al., 2015). Positive staining of NCAM1, SOX1, and NEUROD1 corroborated the compiled RNA-seq data from P-Os (Figures 6C-6E and S6F) and confirmed the presence of a neural/NE signature. Although NEUROD1 expression was primarily localized to the cytoplasm, import of NEUROD1 to the nucleus has known regulatory dependencies, including dimerization with partner proteins (Mehmood et al., 2009) or glucose-dependent phosphorylation (Andrali et al., 2007). Taken together, these data support a prominent off-target neural and NE signature in P-Os.

DISCUSSION

Our comprehensive analysis of major protocols for CM and HC engineering resulted in several key observations that

⁽B) Heatmap of HC and neuronal marker gene expression for the same studies as in (A). Heatmap color scale: per-gene Z score of log-transformed TPM.

⁽C–E) IF staining for (C) the NE marker NCAM1 (green) and the HC marker albumin (ALB; red), (D) the neuronal marker SOX1 (green) and the HC marker SERPINA1 (red), and (E) the neuronal marker NEUROD1 (green) and the CL marker KRT7 (red). Blue, DAPI. Scale bars, 100 μm. See also Figure S6.



are relevant to the CFE field. For CM engineering, we found that two methods of purification at the later stages of differentiation proved especially effective: (1) metabolic selection via glucose deprivation and sodium DL-lactate supplementation and (2) cell sorting for myosin light chain 2 positivity. These purification methods were non-redundant because differentiated MLC2v⁺ CMs retained a glucose catabolism signature more similar to the metabolic profile of CMs that did not undergo metabolic selection, suggesting that a combination of the two techniques could achieve even higher classification scores.

In examining variability within and across CM derivation studies, we observed that studies with higher mean classification scores generally achieved a higher consistency (via lower intra-study SD). At the inter-study level, the ability of a protocol to produce the most highly classifying CMs did not relate to protocol variability, with comparable top-scoring samples observed across protocols irrespective of SD. In contrast, across HC and hepatic organoid engineering studies, at the intra-lab and inter-lab levels, low variability was not associated with high PACNet scores. Our broad assessment of transcriptional fidelity of CFE protocols was not designed to determine the contributors to intra- and inter-study variability. However, on the CM side, protocols with high intra-study variability tended to use PSCs originating from a range of sources, including dermal fibroblasts, mesenchymal stem cells, and peripheral blood mononuclear cells. Further investigation of cell of origin and other potential contributors to protocol variability will facilitate greater consistency in CFE protocols.

Our analysis also identified several recurring off-target signatures in CM and HC engineering studies. Most notably, we observed joint neural and NE signatures in primary liver- and primary HC-derived organoids. We confirmed that this signature was not idiosyncratic to our analytical method because we validated the expression of key liver, neural, and NE marker genes via analysis of expression profiles provided in the original studies and by IF staining of liver organoids that we generated following the same protocol. We postulate that CL-related DR may contribute to the neural/NE transcriptional programs that are detected in these organoids. Enrichment of neuron development gene sets has also been observed in primary murine liver organoids (Aloia et al., 2019), consistent with a CL-neural signature relationship. Off-target cell fate signatures could also potentially be explained by lineage biases induced by the unanticipated impact of added growth factors and small-molecule inhibitors. Ectopic organoid culture-specific signatures have precedents in other in vitro contexts as well. For example, endoplasmic reticulum stress and glycolytic stress signatures are known to appear in brain organoids which are not reflected in primary fetal tissue signatures (Bhaduri et al., 2020; Vértesy et al., 2022). Human kidney organoid culture protocols are also known to exhibit unexpected neural signatures (Howden et al., 2019; Liu et al., 2020; Wu et al., 2018), potentially supporting an organoid culture-specific artifactual neural signature. Further work will be necessary to determine specific mechanisms that induce off-target gene expression signatures in organoids and to characterize shared aberrant patterns of intestinal, neural, and other signatures across organoid derivation protocols, which could have broad implications for organoid derivation and maintenance and their applications.

We note several caveats in this study and areas for improving the PACNet platform. First, because PACNet takes as input bulk RNA-seq data for training and query, it is unable to distinguish hybrid signatures from population heterogeneity in query engineered samples. Moreover, we have not demonstrated that PACNet trained on bulk data is able to discern differences between cell subtypes. Computational methods tailored for the analysis of single-cell RNA-seq (scRNA-seq) data, such as Capybara (Kong et al., 2022), should be able to address these issues with adequate training data. As more single-cell RNA-seq studies are performed across diverse CFE protocols and diverse reference cell types (Tabula Muris Consortium, 2020; Tabula Muris Consortium et al., 2018), we can extend PACNet to provide comparisons of single-cell transcriptional studies in CFE. Nonetheless, our bulk analysis still accurately evaluates cross-sample and cross-study performance and detects off-target signatures, whether they arise from hybrid states or population heterogeneity.

Second, PACNet analysis is limited to transcriptional data and does not consider epigenetic, proteomic, post-translational, or functional characteristics. Transcriptional profiles have been reported to have modest correlation with proteomic (de Sousa Abreu et al., 2009) and epigenetic (Jjingo et al., 2012; Starks et al., 2019) profiles. Transcriptional profiling also cannot explicitly measure post-translational events, including ligand-receptor interactions, signal transduction events, and protein-protein interactions, which play crucial roles in regulating cell type identity. Future efforts will be necessary to see how integration of proteomic and epigenetic data types can further improve cell type classification algorithms.

Finally, PACNet was trained using samples from adults; thus, this platform is likely to be less sensitive to engineered populations that are equivalent to embryonic or fetal stages of development. Currently, primary postnatal or fetal samples can be included in analysis to detect on- and off-target signatures relative to the primary adult samples on which PACNet is trained. As more transcriptomic data accrue of developmental stages, especially using scRNA-seq and



single-nucleus RNA-seq, we expect that computational methods that predict the developmental stage of specific tissues and lineages will be readily trained and applied to cell engineering.

We provide PACNet as a web platform (http://cahanlab. org/resources/agnosticCellNet_web/) through which users can browse engineered reference panels or perform analysis and as code that can be downloaded, modified, and executed locally (https://github.com/pcahan1/PACNet). PACNet provides precise and sensitive classification to detect on- and off-target transcriptional signatures and makes predictions for improved expression of CT type-specific TFs. Importantly, PACNet also provides cross-study comparisons among current state-of-the-field CFE protocols for seven major CT types: liver, heart, neuron, skeletal muscle, lung, intestine/colon, and HSPCs. Thus, PACNet will be a valuable resource to the cell engineering community as a tool that allows standard comparison of engineered populations of cells and as a broad database of CFE protocols.

EXPERIMENTAL PROCEDURES

Resource availability

Corresponding author

The corresponding author is Patrick Cahan (patrick.cahan@jhmi.edu).

Materials availability

Primary liver-derived organoids are available upon request to the corresponding author.

Data and code availability

The PACNet web application is available at http://cahanlab.org/resources/agnosticCellNet_web/. Open-source, extensible code for running PACNet is available at https://github.com/pcahan1/PACNet.

RNA-seq preprocessing and adapting author-provided expression data

Publicly available RNA-seq and expression microarray datasets for query and training were curated from the NCBI GEO (Table S1). For studies that did not provide preprocessed gene-by-sample expression matrices, we used the following pipeline. First, adapters and low-quality bases were trimmed from FASTQ files using cutadapt. Trimmed FASTQs were mapped and quantified using Salmon in mapping-based mode to generate a gene-by-sample expression matrix.

Cell/tissue-specific classifier training and validation

Primary human bulk RNA-seq training data were acquired from NCBI GEO (Table S1). FASTQ files were preprocessed into gene-by-sample expression matrices as described in the above pipeline. For each query CT type, an RF classifier was trained on 2/3 of the training samples from each CT type using the TSP algorithm as described previously (Peng et al., 2021; Tan and Cahan, 2019).

Briefly, template matching was used to identify the top 100 genes highly correlating with each CT type. These genes were used as input to a gene pair transformation, and each gene pair was ranked by its ability to discriminate between CT types. Using the top 100 discriminative gene pairs, a gene pair-by-sample binary matrix was constructed. A "random" cell type was generated by shuffling values in the binary matrix, randomly sampling 70 profiles, and appending these to the binary matrix. This matrix was used to train an RF classifier of 2,000 trees, with stratified sampling of 25 samples from each cell type to ensure balanced training among CT types. Validation of the classifier was performed on the remaining 1/3 of the training samples for each CT type and on 60 randomly shuffled expression profiles. Classifier performance was assessed using AUPR.

DE and GSEA

DE analysis for RNA-seq data was performed with DESeq2 (Love et al., 2014). GSEA was performed with the R package Fast GSEA (fGSEA) (Korotkevich et al., 2016), using the C2 and C5 gene sets from the Molecular Signatures Database (Liberzon et al., 2011; Subramanian et al., 2005).

Transcriptional regulator scoring

GRN construction was performed as described previously (Peng et al., 2021), and for each CT type, the GRN was subset based on genes present in all corresponding query samples. For each sample, candidate TFs for improving the classification of its target CT type were scored using the previously described NIS (Cahan et al., 2014; Radley et al., 2017) applied to rank-transformed expression estimates. In brief, the NIS of a TF is defined as follows:

$$NIS_{TF} = n \times Zscore(TF) \times weight_{TF} + \sum_{n=1}^{n} Zscore(target_i) * weight_i$$

where

n = number of genes directly regulated by TF

The NIS function includes an optional parameter weight, whereby the TF and target gene terms will be weighted according to their expression in the target cell type.

Derivation of primary liver organoids

Primary liver organoids were derived as described previously (Broutier et al., 2016; Huch et al., 2015). Donor liver tissue was received submerged in PBS -/- in a 50-mL tube on ice directly after the surgical procedure. Tissue was immediately transferred to a 10-cm Petri dish in cold basal medium (Advanced DMEM/ F-12 with 100 U/mL penicillin, 100 μg/mL streptomycin, 2 mM Glutamax, and 10 mM HEPES). A sterile scalpel was used to finely mince tissue to make cells accessible for digestion. Tissue pieces were transferred to a 15-mL tube and washed twice with wash medium (DMEM with 1% fetal bovine serum (FBS), 100 U/mL penicillin, 100 μg/mL streptomycin, 2 mM Glutamax), with supernatant manually aspirated with a serological pipette after allowing the minced tissue to settle. Tissue was digested with addition of 4 mL digestion solution (Hank's balanced salt solution [HBSS]+/+, 1.25 mg/mL collagenase IV, 0.1 mg/mL DNaseI) on a rotor at 37°C for 30 min. The digested cell suspension was brough



to 15 mL with cold wash medium and passed through a 70-um mesh into a 50-mL tube. Cells were pelleted at 300 \times g for 5 min at 8°C, and the supernatant was gently aspirated. Cells were washed an additional three times in cold wash medium and a third time in cold basal medium. Medium was aspirated gently with a serological pipette, and a fraction of the cells was transferred to cold Matrigel GFR at a volume ratio of 1:3 to reach a final ${\sim}40{,}000$ cells/mL. 25- ${\mu}L$ droplets of Matrigel suspension were distributed into the centers of 48-well-plate wells. Plates were incubated upside down in a tissue culture incubator (37°C, 5% CO₂) for 10-20 min until the Matrigel completely solidified. Cultures were overlaid with isolation medium (basal medium with 1× B27 supplement without vitamin A, 1× N2 supplement, 1.25 mM N-acetylcysteine, 10% (v/v) RSPO1-conditioned medium, 10 mM nicotinamide, 10 nM recombinant human [Leu]-gastrin I, 50 ng/mL recombinant human EGF, 100 ng/mL recombinant human FGF10, 25 ng/mL recombinant human HGF, 10 μM forskolin, 5 μM A83-01, 25 ng/mL recombinant human Noggin, 30% (v/v) Wnt3a-conditioned medium, and 10 µM Y-27632) for 4 days before switching to expansion medium (isolation medium without Noggin, Wnt3A-conditioned medium, or Y-27632), and changing the medium every 3-4 days. Cultures were passaged on day 13 after isolation. The use of primary human hepatocytes for research was approved by ethical committees and informed consent was obtained from donors when appropriate. No personally identifying information has been released.

Passaging of human liver organoids

Organoids were passaged 13 days after the original isolation and every 5–7 days afterward. Organoid cultures were disrupted with a P1000 micropipette and the wells rinsed twice with 500 μ L of cold basal medium to dissolve the Matrigel droplet and transfer the cells to a 15-mL centrifuge tube. Tubes were topped off to 13 mL with cold basal medium and agitated 5 times with a micropipette to completely dissolve the Matrigel. Organoids were spun at 200 × g for 5 min at 8°C and aspirated with 1 mL remaining, then agitated using a micropipette until sufficiently dissociated. Tubes were again topped to 13 mL with basal medium, spun at 200 × g for 5 min at 8°C, and aspirated. Cells were mixed with cold Matrigel to reach a passage ratio of 1:6, and droplets were formed and overlaid as in the isolation procedure but with expansion medium instead of isolation medium.

IF staining and imaging

Whole-mount staining of primary human liver organoids was performed as follows. Glass-bottom plates (Ibidi) containing Matrigel droplet organoid suspensions were rinsed twice with cold PBS –/– (Quality Biological), then fixed in 4% paraformal-dehyde (PFA) (Electron Microscopy Sciences) for 30 min at room temperature (RT); the remaining incubations and washes were performed at RT unless otherwise specified. Wells were rinsed three times with PBS–/– and then permeabilized with 0.3% Triton X-100 for 25 min. Wells were again rinsed three times in PBS–/– and blocked with 5% normal donkey serum (Jackson ImmunoResearch Laboratories) for 45 min, rinsed once in PBS–/–, and incubated overnight at 4°C with primary anti-

bodies in 5% donkey serum in 0.05% Tween 20 in PBS-/-(PBST). A negative control was incubated under the same conditions but with no primary antibodies. Cells were washed with PBST three times for 10 min per wash and then incubated with secondary antibody in PBST for 90 min. Wells were rinsed twice with PBS and then incubated with a 1:1,500 dilution of Hoechst (Invitrogen) in PBST for 10 min before a final 3 washes of 10 min each. The stained cultures were then imaged on a Nikon A1 spectral confocal microscope using z stack scans, which were processed in ImageJ to generate the z projections shown in the figures. The negative control that was incubated with secondary but not primary antibodies was used to set the parameters to determine the background threshold for each channel. Antibody catalog numbers and dilutions are shown in Table S6.

SUPPLEMENTAL INFORMATION

Supplemental information can be found online at https://doi.org/10.1016/j.stemcr.2023.06.008.

AUTHOR CONTRIBUTIONS

E.K.W.L curated data, wrote code, performed analysis, and wrote the manuscript. J.J.V. performed experiments and edited the manuscript. D.P. wrote code and edited the manuscript. C.K. guided analysis and edited the manuscript. M.R.E. oversaw experiments, guided analysis, and edited the manuscript. P.C. conceived and oversaw the project, guided analysis, and edited the manuscript.

ACKNOWLEDGMENTS

E.K.W.L. is supported by the NCI under award F31CA250489 and by the ARCS Fellowship through the JCM Foundation. M.R.E. is supported by R01s from the NIBIB (EB028532) and the NHLBI (HL141805), by NSF CBET award 2134999, and by the Pittsburgh Liver Research Center (P30DK120531). P.C. is supported by EB028532 and by the NIGMS (R35GM124725). The graphical abstract was created at Biorender.com.

CONFLICT OF INTERESTS

M.R.E., J.J.V., and P.C. have a patent (US20210254012A1) for the organoids analyzed from Velazquez et al. (2021). P.C. is an associate editor of *Stem Cell Reports*.

DECLARATION OF GENERATIVE AI AND AI-ASSISTED TECHNOLOGIES IN THE WRITING PROCESS

During the preparation of this work, the authors used ChatGPT version 4.0 to reduce the character count of the Highlights to meet journal length limits. After using this tool, the authors reviewed and edited the content as needed and take full responsibility for the content of the publication.

Received: September 7, 2022 Revised: June 16, 2023 Accepted: June 17, 2023 Published: July 20, 2023



REFERENCES

Abeyta, M.J., Clark, A.T., Rodriguez, R.T., Bodnar, M.S., Pera, R.A.R., and Firpo, M.T. (2004). Unique gene expression signatures of independently-derived human embryonic stem cell lines. Hum. Mol. Genet. *13*, 601–608. https://doi.org/10.1093/hmg/ddh068.

Akazawa, H., and Komuro, I. (2005). Cardiac transcription factor Csx/Nkx2-5: Its role in cardiac development and diseases. Pharmacol. Ther. *107*, 252–268. https://doi.org/10.1016/j.pharmthera. 2005.03.005.

Akbari, S., Sevinç, G.G., Ersoy, N., Basak, O., Kaplan, K., Sevinç, K., Ozel, E., Sengun, B., Enustun, E., Ozcimen, B., et al. (2019). Robust, Long-Term Culture of Endoderm-Derived Hepatic Organoids for Disease Modeling. Stem Cell Rep. *13*, 627–641. https://doi.org/10.1016/j.stemcr.2019.08.007.

Aloia, L., McKie, M.A., Vernaz, G., Cordero-Espinoza, L., Aleksieva, N., van den Ameele, J., Antonica, F., Font-Cunill, B., Raven, A., Aiese Cigliano, R., et al. (2019). Epigenetic remodelling licences adult cholangiocytes for organoid formation and liver regeneration. Nat. Cell Biol. *21*, 1321–1333. https://doi.org/10.1038/s41556-019-0402-6.

Alvaro, D., Mancino, M.G., Glaser, S., Gaudio, E., Marzioni, M., Francis, H., and Alpini, G. (2007). Proliferating cholangiocytes: a neuroendocrine compartment in the diseased liver. Gastroenterology *132*, 415–431. https://doi.org/10.1053/j.gastro.2006.07.023.

Andersen, P., Tampakakis, E., Jimenez, D.V., Kannan, S., Miyamoto, M., Shin, H.K., Saberi, A., Murphy, S., Sulistio, E., Chelko, S.P., and Kwon, C. (2018). Precardiac organoids form two heart fields via Bmp/Wnt signaling. Nat. Commun. *9*, 3140. https://doi.org/10.1038/s41467-018-05604-8.

Andrali, S.S., Qian, Q., and Ozcan, S. (2007). Glucose mediates the translocation of NeuroD1 by O-linked glycosylation. J. Biol. Chem. *282*, 15589–15596. https://doi.org/10.1074/jbc.M701762200.

Avior, Y., Biancotti, J.C., and Benvenisty, N. (2015a). TeratoScore: Assessing the Differentiation Potential of Human Pluripotent Stem Cells by Quantitative Expression Analysis of Teratomas. Stem Cell Rep. 4, 967–974. https://doi.org/10.1016/j.stemcr. 2015.05.006.

Avior, Y., Levy, G., Zimerman, M., Kitsberg, D., Schwartz, R., Sadeh, R., Moussaieff, A., Cohen, M., Itskovitz-Eldor, J., and Nahmias, Y. (2015b). Microbial-derived lithocholic acid and vitamin K2 drive the metabolic maturation of pluripotent stem cells-derived and fetal hepatocytes. Hepatology *62*, 265–278. https://doi.org/10.1002/hep.27803.

Banales, J.M., Huebert, R.C., Karlsen, T., Strazzabosco, M., LaRusso, N.F., and Gores, G.J. (2019). Cholangiocyte pathobiology. Nat. Rev. Gastroenterol. Hepatol. *16*, 269–281. https://doi.org/10.1038/s41575-019-0125-y.

Bhaduri, A., Andrews, M.G., Mancia Leon, W., Jung, D., Shin, D., Allen, D., Jung, D., Schmunk, G., Haeussler, M., Salma, J., et al. (2020). Cell stress in cortical organoids impairs molecular subtype specification. Nature *578*, 142–148. https://doi.org/10.1038/s41586-020-1962-0.

Blache, P., van de Wetering, M., Duluc, I., Domon, C., Berta, P., Freund, J.-N., Clevers, H., and Jay, P. (2004). SOX9 is an intestine crypt transcription factor, is regulated by the Wnt pathway, and re-

presses the CDX2 and MUC2 genes. J. Cell Biol. *166*, 37–47. https://doi.org/10.1083/jcb.200311021.

Boon, R., Kumar, M., Tricot, T., Elia, I., Ordovas, L., Jacobs, F., One, J., De Smedt, J., Eelen, G., Bird, M., et al. (2020). Amino acid levels determine metabolism and CYP450 function of hepatocytes and hepatoma cell lines. Nat. Commun. *11*, 1393. https://doi.org/10.1038/s41467-020-15058-6.

Brivanlou, A.H., Gage, F.H., Jaenisch, R., Jessell, T., Melton, D., and Rossant, J. (2003). Stem cells. Setting standards for human embryonic stem cells. Science *300*, 913–916. https://doi.org/10.1126/science.1082940.

Broutier, L., Andersson-Rolf, A., Hindley, C.J., Boj, S.F., Clevers, H., Koo, B.-K., and Huch, M. (2016). Culture and establishment of self-renewing human and mouse adult liver and pancreas 3D organoids and their genetic manipulation. Nat. Protoc. *11*, 1724–1743. https://doi.org/10.1038/nprot.2016.097.

Buikema, J.W., Van Der Meer, P., Sluijter, J.P.G., and Domian, I.J. (2013). Concise review: Engineering myocardial tissue: the convergence of stem cells biology and tissue engineering technology. Stem Cell. *31*, 2587–2598. https://doi.org/10.1002/stem.1467.

Burridge, P.W., Matsa, E., Shukla, P., Lin, Z.C., Churko, J.M., Ebert, A.D., Lan, F., Diecke, S., Huber, B., Mordwinkin, N.M., et al. (2014). Chemically defined generation of human cardiomyocytes. Nat. Methods *11*, 855–860. https://doi.org/10.1038/nmeth.2999.

Burridge, P.W., Holmström, A., and Wu, J.C. (2015). Chemically defined culture and cardiomyocyte differentiation of human pluripotent stem cells. Curr. Protoc. Hum. Genet. *87*, 21.3.1–21.3.15. https://doi.org/10.1002/0471142905.hg2103s87.

Cahan, P., Li, H., Morris, S.A., Lummertz da Rocha, E., Daley, G.Q., and Collins, J.J. (2014). CellNet: network biology applied to stem cell engineering. Cell *158*, 903–915. https://doi.org/10.1016/j.cell.2014.07.020.

Carpentier, A., Sheldon, J., Vondran, F.W.R., Brown, R.J., and Pietschmann, T. (2020). Efficient acute and chronic infection of stem cell-derived hepatocytes by hepatitis C virus. Gut *69*, 1659–1666. https://doi.org/10.1136/gutjnl-2019-319354.

Chung, S., Dzeja, P.P., Faustino, R.S., Perez-Terzic, C., Behfar, A., and Terzic, A. (2007). Mitochondrial oxidative metabolism is required for the cardiac differentiation of stem cells. Nat. Clin. Pract. Cardiovasc. Med. *4* (*Suppl 1*), S60–S67. https://doi.org/10.1038/ncpcardio0766.

Davis, R.L., Weintraub, H., and Lassar, A.B. (1987). Expression of a single transfected cDNA converts fibroblasts to myoblasts. Cell *51*, 987–1000. https://doi.org/10.1016/0092-8674(87)90585-x.

Deaton, A.M., Sulem, P., Nioi, P., Benonisdottir, S., Ward, L.D., Davidsson, O.B., Lao, S., Helgadottir, A., Fan, F., Jensson, B.O., et al. (2018). A rare missense variant in NR1H4 associates with lower cholesterol levels. Commun. Biol. *1*, 14. https://doi.org/10.1038/s42003-018-0015-9.

Drakhlis, L., Biswanath, S., Farr, C.-M., Lupanow, V., Teske, J., Ritzenhoff, K., Franke, A., Manstein, F., Bolesani, E., Kempf, H., et al. (2021). Human heart-forming organoids recapitulate early heart and foregut development. Nat. Biotechnol. *39*, 737–746. https://doi.org/10.1038/s41587-021-00815-9.



Du, Y., Wang, J., Jia, J., Song, N., Xiang, C., Xu, J., Hou, Z., Su, X., Liu, B., Jiang, T., et al. (2014). Human hepatocytes with drug metabolic function induced from fibroblasts by lineage reprogramming. Cell Stem Cell 14, 394–403. https://doi.org/10.1016/j.stem.2014. 01.008.

Ehrlich, A., Ayyash, M., Zimerman, M., Schwartz, R., Hofree, M., and Nahmias, Y. Postnatal Lipids Drive Hepatocyte Maturation

Ehrlich, L., Scrushy, M., Meng, F., Lairmore, T.C., Alpini, G., and Glaser, S. (2018). Biliary epithelium: A neuroendocrine compartment in cholestatic liver disease. Clin. Res. Hepatol. Gastroenterol. 42, 296-305. https://doi.org/10.1016/j.clinre.2018.03.009.

Estarás, C., Hsu, H.-T., Huang, L., and Jones, K.A. (2017). YAP repression of the WNT3 gene controls hESC differentiation along the cardiac mesoderm lineage. Genes Dev. 31, 2250-2263. https://doi.org/10.1101/gad.307512.117.

Evans, M.J., and Kaufman, M.H. (1981). Establishment in culture of pluripotential cells from mouse embryos. Nature 292, 154-156. https://doi.org/10.1038/292154a0.

Gao, Y., Zhang, X., Zhang, L., Cen, J., Ni, X., Liao, X., Yang, C., Li, Y., Chen, X., Zhang, Z., et al. (2017). Distinct Gene Expression and Epigenetic Signatures in Hepatocyte-like Cells Produced by Different Strategies from the Same Donor. Stem Cell Rep. 9, 1813-1824. https://doi.org/10.1016/j.stemcr.2017.10.019.

Geman, D., d'Avignon, C., Naiman, D.Q., and Winslow, R.L. (2004). Classifying gene expression profiles from pairwise mRNA comparisons. Stat. Appl. Genet. Mol. Biol. 3, Article19. https:// doi.org/10.2202/1544-6115.1071.

Hannan, N.R.F., Segeritz, C.-P., Touboul, T., and Vallier, L. (2013). Production of hepatocyte-like cells from human pluripotent stem cells. Nat. Protoc. 8, 430-437. https://doi.org/10.1038/ nprot.2012.153.

Howden, S.E., Vanslambrouck, J.M., Wilson, S.B., Tan, K.S., and Little, M.H. (2019). Reporter-based fate mapping in human kidney organoids confirms nephron lineage relationships and reveals synchronous nephron formation. EMBO Rep. 20, e47483. https://doi. org/10.15252/embr.201847483.

Hsu, H.-T., Estarás, C., Huang, L., and Jones, K.A. (2018). Specifying the anterior primitive streak by modulating YAP1 levels in human pluripotent stem cells. Stem Cell Rep. 11, 1357-1364. https://doi. org/10.1016/j.stemcr.2018.10.013.

Huch, M., Dorrell, C., Boj, S.F., van Es, J.H., Li, V.S.W., van de Wetering, M., Sato, T., Hamer, K., Sasaki, N., Finegold, M.J., et al. (2013). In vitro expansion of single Lgr5+ liver stem cells induced by Wnt-driven regeneration. Nature 494, 247-250. https://doi. org/10.1038/nature11826.

Huch, M., Gehart, H., van Boxtel, R., Hamer, K., Blokzijl, F., Verstegen, M.M.A., Ellis, E., van Wenum, M., Fuchs, S.A., de Ligt, J., et al. (2015). Long-term culture of genome-stable bipotent stem cells from adult human liver. Cell 160, 299-312. https://doi.org/10. 1016/j.cell.2014.11.050.

Hu, H., Gehart, H., Artegiani, B., LÖpez-Iglesias, C., Dekkers, F., Basak, O., van Es, J., Chuva de Sousa Lopes, S.M., Begthel, H., Korving, J., et al. (2018). Long-Term Expansion of Functional Mouse and Human Hepatocytes as 3D Organoids. Cell 175, 1591-1606.e19. https://doi.org/10.1016/j.cell.2018.11.013.

Ieda, M., Fu, J.-D., Delgado-Olguin, P., Vedantham, V., Hayashi, Y., Bruneau, B.G., and Srivastava, D. (2010). Direct reprogramming of fibroblasts into functional cardiomyocytes by defined factors. Cell 142, 375-386. https://doi.org/10.1016/j.cell.2010.07.002.

International Stem Cell Initiative (2018). Assessment of established techniques to determine developmental and malignant potential of human pluripotent stem cells. Nat. Commun. 9, 1925. https://doi.org/10.1038/s41467-018-04011-3.

Jin, M., Yi, X., Liao, W., Chen, Q., Yang, W., Li, Y., Li, S., Gao, Y., Peng, Q., and Zhou, S. (2021). Advancements in stem cell-derived hepatocyte-like cell models for hepatotoxicity testing. Stem Cell Res. Ther. 12, 84. https://doi.org/10.1186/s13287-021-02152-9.

Jjingo, D., Conley, A.B., Yi, S.V., Lunyak, V.V., and Jordan, I.K. (2012). On the presence and role of human gene-body DNA methylation. Oncotarget 3, 462-474. https://doi.org/10.18632/ oncotarget.497.

Kang, S., Chen, X., Gong, S., Yu, P., Yau, S., Su, Z., Zhou, L., Yu, J., Pan, G., and Shi, L. (2017). Characteristic analyses of a neural differentiation model from iPSC-derived neuron according to morphology, physiology, and global gene expression pattern. Sci. Rep. 7, 12233. https://doi.org/10.1038/s41598-017-12452-x.

Karakikes, I., Ameen, M., Termglinchan, V., and Wu, J.C. (2015). Human induced pluripotent stem cell-derived cardiomyocytes: insights into molecular, cellular, and functional phenotypes. Circ. Res. 117, 80-88. https://doi.org/10.1161/CIRCRESAHA. 117.305365.

Kim, K., Doi, A., Wen, B., Ng, K., Zhao, R., Cahan, P., Kim, J., Aryee, M.J., Ji, H., Ehrlich, L.I.R., et al. (2010). Epigenetic memory in induced pluripotent stem cells. Nature 467, 285-290. https://doi. org/10.1038/nature09342.

Kong, W., Fu, Y.C., Holloway, E.M., Garipler, G., Yang, X., Mazzoni, E.O., and Morris, S.A. (2022). Capybara: A computational tool to measure cell identity and fate transitions. Cell Stem Cell 29, 635-649.e11. https://doi.org/10.1016/j.stem.2022.03.001.

Kopec, A.K., and Luyendyk, J.P. (2014). Coagulation in liver toxicity and disease: role of hepatocyte tissue factor. Thromb. Res. 133, S57–S59. https://doi.org/10.1016/j.thromres. 2014.03.023.

Korotkevich, G., Sukhov, V., Budin, N., Shpak, B., Artyomov, M.N., and Sergushichev, A. (2016). Fast gene set enrichment analysis. Preprint at bioRxiv. https://doi.org/10.1101/060012.

Kubo, A., Shinozaki, K., Shannon, J.M., Kouskoff, V., Kennedy, M., Woo, S., Fehling, H.J., and Keller, G. (2004). Development of definitive endoderm from embryonic stem cells in culture. Development 131, 1651-1662. https://doi.org/10.1242/dev.01044.

Lee, J.H., Protze, S.I., Laksman, Z., Backx, P.H., and Keller, G.M. (2017). Human Pluripotent Stem Cell-Derived Atrial and Ventricular Cardiomyocytes Develop from Distinct Mesoderm Populations. Cell Stem Cell 21, 179–194.e4. https://doi.org/10.1016/j.stem. 2017.07.003.

Lian, X., Hsiao, C., Wilson, G., Zhu, K., Hazeltine, L.B., Azarin, S.M., Raval, K.K., Zhang, J., Kamp, T.J., and Palecek, S.P. (2012). Robust cardiomyocyte differentiation from human pluripotent stem cells via temporal modulation of canonical Wnt signaling.



Proc. Natl. Acad. Sci. USA 109, E1848–E1857. https://doi.org/10. 1073/pnas.1200250109.

Lian, X., Zhang, J., Azarin, S.M., Zhu, K., Hazeltine, L.B., Bao, X., Hsiao, C., Kamp, T.J., and Palecek, S.P. (2013). Directed cardiomyocyte differentiation from human pluripotent stem cells by modulating Wnt/β-catenin signaling under fully defined conditions. Nat. Protoc. 8, 162–175. https://doi.org/10.1038/nprot.2012.150.

Liberzon, A., Subramanian, A., Pinchback, R., Thorvaldsdóttir, H., Tamayo, P., and Mesirov, J.P. (2011). Molecular signatures database (MSigDB) 3.0. Bioinformatics 27, 1739–1740. https://doi.org/10. 1093/bioinformatics/btr260.

Liu, E., Radmanesh, B., Chung, B.H., Donnan, M.D., Yi, D., Dadi, A., Smith, K.D., Himmelfarb, J., Li, M., Freedman, B.S., and Lin, J. (2020). Profiling APOL1 Nephropathy Risk Variants in Genome-Edited Kidney Organoids with Single-Cell Transcriptomics. Kidney360 1, 203-215. https://doi.org/10.34067/kid.0000422019.

Lopaschuk, G.D., and Jaswal, J.S. (2010). Energy metabolic phenotype of the cardiomyocyte during development, differentiation, and postnatal maturation. J. Cardiovasc. Pharmacol. 56, 130-140. https://doi.org/10.1097/FJC.0b013e3181e74a14.

Love, M.I., Huber, W., and Anders, S. (2014). Moderated estimation of fold change and dispersion for RNA-seq data with DESeq2. Genome Biol. 15, 550. https://doi.org/10.1186/s13059-014-0550-8.

Lo, E.K.W., and Cahan, P. (2019). Cell Fate Engineering Tools for iPSC Disease Modeling. Methods Mol. Biol. 1975, 427-454. https://doi.org/10.1007/978-1-4939-9224-9_19.

Martin, G.R. (1981). Isolation of a pluripotent cell line from early mouse embryos cultured in medium conditioned by teratocarcinoma stem cells. Proc. Natl. Acad. Sci. USA 78, 7634-7638. https://doi.org/10.1073/pnas.78.12.7634.

Ma, X., Duan, Y., Tschudy-Seney, B., Roll, G., Behbahan, I.S., Ahuja, T.P., Tolstikov, V., Wang, C., McGee, J., Khoobyari, S., et al. (2013). Highly efficient differentiation of functional hepatocytes from human induced pluripotent stem cells. Stem Cells Transl. Med. 2, 409–419. https://doi.org/10.5966/sctm.2012-0160.

Mehmood, R., Yasuhara, N., Oe, S., Nagai, M., and Yoneda, Y. (2009). Synergistic nuclear import of NeuroD1 and its partner transcription factor, E47, via heterodimerization. Exp. Cell Res. 315, 1639–1652. https://doi.org/10.1016/j.yexcr.2009.02.025.

Morris, S.A., Cahan, P., Li, H., Zhao, A.M., San Roman, A.K., Shivdasani, R.A., Collins, J.J., and Daley, G.Q. (2014). Dissecting engineered cell types and enhancing cell fate conversion via CellNet. Cell 158, 889-902. https://doi.org/10.1016/j.cell.2014.07.021.

Müller, F.J., Schuldt, B.M., Williams, R., Mason, D., Altun, G., Papapetrou, E.P., Danner, S., Goldmann, J.E., Herbst, A., Schmidt, N.O., et al. (2011). A bioinformatic assay for pluripotency in human cells. Nat. Methods 8, 315-317. https://doi.org/10.1038/ nmeth.1580.

Munshi, M.K., Priester, S., Gaudio, E., Yang, F., Alpini, G., Mancinelli, R., Wise, C., Meng, F., Franchitto, A., Onori, P., and Glaser, S.S. (2011). Regulation of biliary proliferation by neuroendocrine factors: implications for the pathogenesis of cholestatic liver diseases. Am. J. Pathol. 178, 472-484. https://doi.org/10.1016/j.ajpath.2010.09.043.

Nagy, A., Gócza, E., Diaz, E.M., Prideaux, V.R., Iványi, E., Markkula, M., and Rossant, J. (1990). Embryonic stem cells alone are able to support fetal development in the mouse. Development 110, 815-821. https://doi.org/10.1242/dev.110.3.815.

Osafune, K., Caron, L., Borowiak, M., Martinez, R.J., Fitz-Gerald, C.S., Sato, Y., Cowan, C.A., Chien, K.R., and Melton, D.A. (2008). Marked differences in differentiation propensity among human embryonic stem cell lines. Nat. Biotechnol. 26, 313-315. https:// doi.org/10.1038/nbt1383.

Peng, D., Gleyzer, R., Tai, W.-H., Kumar, P., Bian, Q., Isaacs, B., da Rocha, E.L., Cai, S., DiNapoli, K., Huang, F.W., and Cahan, P. (2021). Evaluating the transcriptional fidelity of cancer models. Genome Med. 13, 73. https://doi.org/10.1186/s13073-021-00888-w.

Pleguezuelos-Manzano, C., Puschhof, J., van den Brink, S., Geurts, V., Beumer, J., and Clevers, H. (2020). Establishment and Culture of Human Intestinal Organoids Derived from Adult Stem Cells. Curr. Protoc. Immunol. 130, e106. https://doi.org/10.1002/cpim.106.

Qin, J., Chang, M., Wang, S., Liu, Z., Zhu, W., Wang, Y., Yan, F., Li, J., Zhang, B., Dou, G., et al. (2016). Connexin 32-mediated cell-cell communication is essential for hepatic differentiation from human embryonic stem cells. Sci. Rep. 6, 37388. https://doi.org/10. 1038/srep37388.

Radley, A.H., Schwab, R.M., Tan, Y., Kim, J., Lo, E.K.W., and Cahan, P. (2017). Assessment of engineered cells using CellNet and RNAseq. Nat. Protoc. 12, 1089-1102. https://doi.org/10.1038/nprot. 2017.022.

Robinton, D.A., and Daley, G.Q. (2012). The promise of induced pluripotent stem cells in research and therapy. Nature 481, 295-305. https://doi.org/10.1038/nature10761.

Roost, M.S., van Iperen, L., Ariyurek, Y., Buermans, H.P., Arindrarto, W., Devalla, H.D., Passier, R., Mummery, C.L., Carlotti, F., de Koning, E.J.P., et al. (2015). Keygenes, a tool to probe tissue differentiation using a human fetal transcriptional atlas. Stem Cell Rep. 4, 1112-1124. https://doi.org/10.1016/j.stemcr.2015.05.002.

Rossi, G., Broguiere, N., Miyamoto, M., Boni, A., Guiet, R., Girgin, M., Kelly, R.G., Kwon, C., and Lutolf, M.P. (2021). Capturing cardiogenesis in gastruloids. Cell Stem Cell 28, 230-240.e6. https:// doi.org/10.1016/j.stem.2020.10.013.

Sagi, I., De Pinho, J.C., Zuccaro, M.V., Atzmon, C., Golan-Lev, T., Yanuka, O., Prosser, R., Sadowy, A., Perez, G., Cabral, T., et al. (2019). Distinct imprinting signatures and biased differentiation of human androgenetic and parthenogenetic embryonic stem cells. Cell Stem Cell 25, 419-432.e9. https://doi.org/10.1016/j. stem.2019.06.013.

Schwartz, R.E., Fleming, H.E., Khetani, S.R., and Bhatia, S.N. (2014). Pluripotent stem cell-derived hepatocyte-like cells. Biotechnol. Adv. 32, 504–513. https://doi.org/10.1016/j.biotechadv. 2014.01.003.

Scott, C.E., Wynn, S.L., Sesay, A., Cruz, C., Cheung, M., Gomez Gaviro, M.-V., Booth, S., Gao, B., Cheah, K.S.E., Lovell-Badge, R., and Briscoe, J. (2010). SOX9 induces and maintains neural stem cells. Nat. Neurosci. 13, 1181-1189. https://doi.org/10.1038/ nn.2646.



de Sousa Abreu, R., Penalva, L.O., Marcotte, E.M., and Vogel, C. (2009). Global signatures of protein and mRNA expression levels. Mol. Biosyst. 5, 1512–1526. https://doi.org/10.1039/b908315d.

Starks, R.R., Biswas, A., Jain, A., and Tuteja, G. (2019). Combined analysis of dissimilar promoter accessibility and gene expression profiles identifies tissue-specific genes and actively repressed networks. Epigenet. Chromatin 12, 16. https://doi.org/10.1186/ s13072-019-0260-2.

Strober, B.J., Elorbany, R., Rhodes, K., Krishnan, N., Tayeb, K., Battle, A., and Gilad, Y. (2019). Dynamic genetic regulation of gene expression during cellular differentiation. Science 364, 1287-1290. https://doi.org/10.1126/science.aaw0040.

Subramanian, A., Tamayo, P., Mootha, V.K., Mukherjee, S., Ebert, B.L., Gillette, M.A., Paulovich, A., Pomeroy, S.L., Golub, T.R., Lander, E.S., and Mesirov, J.P. (2005). Gene set enrichment analysis: a knowledge-based approach for interpreting genome-wide expression profiles. Proc. Natl. Acad. Sci. USA 102, 15545-15550. https://doi.org/10.1073/pnas.0506580102.

Sun, W., Cornwell, A., Li, J., Peng, S., Osorio, M.J., Aalling, N., Wang, S., Benraiss, A., Lou, N., Goldman, S.A., and Nedergaard, M. (2017). SOX9 Is an Astrocyte-Specific Nuclear Marker in the Adult Brain Outside the Neurogenic Regions. J. Neurosci. 37, 4493-4507. https://doi.org/10.1523/JNEUROSCI.3199-16.2017.

Tabula Muris Consortium (2020). A single-cell transcriptomic atlas characterizes ageing tissues in the mouse. Nature 583, 590-595. https://doi.org/10.1038/s41586-020-2496-1.

Tabula Muris Consortium; Overall coordination; Logistical coordination; Organ collection and processing; Library preparation and sequencing; Computational data analysis; Cell type annotation; Writing group; Supplemental text writing group; Principal investigators (2018). Single-cell transcriptomics of 20 mouse organs creates a Tabula Muris. Nature 562, 367-372. https://doi.org/10. 1038/s41586-018-0590-4.

Takahashi, K., and Yamanaka, S. (2006). Induction of pluripotent stem cells from mouse embryonic and adult fibroblast cultures by defined factors. Cell 126, 663-676. https://doi.org/10.1016/j. cell.2006.07.024.

Takahashi, K., Tanabe, K., Ohnuki, M., Narita, M., Ichisaka, T., Tomoda, K., and Yamanaka, S. (2007). Induction of pluripotent stem cells from adult human fibroblasts by defined factors. Cell 131, 861-872. https://doi.org/10.1016/j.cell.2007.11.019.

Tan, Y., and Cahan, P. (2019). SingleCellNet: A Computational Tool to Classify Single Cell RNA-Seq Data Across Platforms and Across Species. Cell Syst. 9, 207-213.e2. https://doi.org/10.1016/j.cels. 2019.06.004.

Thomson, J.A., Itskovitz-Eldor, J., Shapiro, S.S., Waknitz, M.A., Swiergiel, J.J., Marshall, V.S., and Jones, J.M. (1998). Embryonic stem cell lines derived from human blastocysts. Science 282, 1145–1147. https://doi.org/10.1126/science.282.5391.1145.

Tohyama, S., Hattori, F., Sano, M., Hishiki, T., Nagahata, Y., Matsuura, T., Hashimoto, H., Suzuki, T., Yamashita, H., Satoh, Y., et al. (2013). Distinct metabolic flow enables large-scale purification of mouse and human pluripotent stem cell-derived cardiomyocytes. Cell Stem Cell 12, 127-137. https://doi.org/10.1016/j. stem.2012.09.013.

Toivonen, S., Lundin, K., Balboa, D., Ustinov, J., Tamminen, K., Palgi, J., Trokovic, R., Tuuri, T., and Otonkoski, T. (2013). Activin A and Wnt-dependent specification of human definitive endoderm cells. Exp. Cell Res. 319, 2535-2544. https://doi.org/10. 1016/j.yexcr.2013.07.007.

Touboul, T., Chen, S., To, C.C., Mora-Castilla, S., Sabatini, K., Tukey, R.H., and Laurent, L.C. (2016). Stage-specific regulation of the WNT/β-catenin pathway enhances differentiation of hESCs into hepatocytes. J. Hepatol. 64, 1315–1326. https://doi.org/10. 1016/j.jhep.2016.02.028.

Tsankov, A.M., Akopian, V., Pop, R., Chetty, S., Gifford, C.A., Daheron, L., Tsankova, N.M., and Meissner, A. (2015). A qPCR ScoreCard quantifies the differentiation potential of human pluripotent stem cells. Nat. Biotechnol. 33, 1182-1192. https:// doi.org/10.1038/nbt.3387.

Velazquez, J.J., LeGraw, R., Moghadam, F., Tan, Y., Kilbourne, J., Maggiore, J.C., Hislop, J., Liu, S., Cats, D., Chuva de Sousa Lopes, S.M., et al. (2021). Gene regulatory network analysis and engineering directs development and vascularization of multilineage human liver organoids. Cell Syst. 12, 41-55.e11. https://doi.org/10. 1016/j.cels.2020.11.002.

Vértesy, Á., Eichmüller, O.L., Naas, J., Novatchkova, M., Esk, C., Balmaña, M., Ladstaetter, S., Bock, C., von Haeseler, A., and Knoblich, J.A. (2022). Gruffi: an algorithm for computational removal of stressed cells from brain organoid transcriptomic datasets. EMBO J. 41, e111118. https://doi.org/10.15252/embj.2022111118.

Wang, S., Wang, X., Tan, Z., Su, Y., Liu, J., Chang, M., Yan, F., Chen, J., Chen, T., Li, C., et al. (2019). Human ESC-derived expandable hepatic organoids enable therapeutic liver repopulation and pathophysiological modeling of alcoholic liver injury. Cell Res. 29, 1009-1026. https://doi.org/10.1038/s41422-019-0242-8.

Wang, Y., Qin, J., Wang, S., Zhang, W., Duan, J., Zhang, J., Wang, X., Yan, F., Chang, M., Liu, X., et al. (2016). Conversion of Human Gastric Epithelial Cells to Multipotent Endodermal Progenitors using Defined Small Molecules. Cell Stem Cell 19, 449–461. https:// doi.org/10.1016/j.stem.2016.06.006.

Wichterle, H., Lieberam, I., Porter, J.A., and Jessell, T.M. (2002). Directed differentiation of embryonic stem cells into motor neurons. Cell 110, 385–397. https://doi.org/10.1016/s0092-8674(02) 00835-8.

Wu, H., Uchimura, K., Donnelly, E.L., Kirita, Y., Morris, S.A., and Humphreys, B.D. (2018). Comparative Analysis and Refinement of Human PSC-Derived Kidney Organoid Differentiation with Single-Cell Transcriptomics. Cell Stem Cell 23, 869–881.e8. https://doi.org/10.1016/j.stem.2018.10.010.

Xie, B., Sun, D., Du, Y., Jia, J., Sun, S., Xu, J., Liu, Y., Xiang, C., Chen, S., Xie, H., et al. (2019). A two-step lineage reprogramming strategy to generate functionally competent human hepatocytes from fibroblasts. Cell Res. 29, 696-710. https://doi.org/10.1038/s41422-019-0196-x.

Yang, L., Soonpaa, M.H., Adler, E.D., Roepke, T.K., Kattman, S.J., Kennedy, M., Henckaerts, E., Bonham, K., Abbott, G.W., Linden, R.M., et al. (2008). Human cardiovascular progenitor cells develop from a KDR+ embryonic-stem-cell-derived population. Nature 453, 524-528. https://doi.org/10.1038/nature06894.



Zhang, J., Tao, R., Campbell, K.F., Carvalho, J.L., Ruiz, E.C., Kim, G.C., Schmuck, E.G., Raval, A.N., da Rocha, A.M., Herron, T.J., et al. (2019). Functional cardiac fibroblasts derived from human pluripotent stem cells via second heart field progenitors. Nat. Commun. 10, 2238. https://doi.org/10.1038/s41467-019-09831-5.

Zhao, Y., Rafatian, N., Feric, N.T., Cox, B.J., Aschar-Sobbi, R., Wang, E.Y., Aggarwal, P., Zhang, B., Conant, G., Ronaldson-Bouchard, K., et al. (2019). A Platform for Generation of Chamber-Specific Cardiac Tissues and Disease Modeling. Cell 176, 913-927.e18. https://doi.org/10.1016/j.cell.2018.11.042.